CrossMark

The Diversity of Cold Worlds: Age and Characterization of the Exoplanet COCONUTS-2 b

Rocio Kiman[1] , Charles A. Beichman[1,2] , Azul Ruiz Diaz[3] , Jacqueline K. Faherty[3] , Brianna Lacy[4] , Genaro Suárez[3] ,
Federico Marocco[2] , J. Davy Kirkpatrick[2] , Jonathan Gagné[5,6] , Jessica Copeland[7] , Ben Burningham[7] ,
Niall Whiteford[3] , Melanie J. Rowland[8] , Daniella C. Bardalez Gagliuffi[9] , Johanna M. Vos[3,10] , Adam C. Schneider[11] ,
Eileen C. Gonzales[12] , Sherelyn Alejandro Merchan[3,13] , Austin Rothermich[3,13,14,15] , Richard Smart[16] ,
Edgardo Costa[17] , and Rene A. Mendez[17]

[1] Department of Astronomy, California Institute of Technology, Pasadena, CA 91125, USA; rociokiman@gmail.com
[2] Infrared Processing and Analysis Center, California Institute of Technology, 1200 East California Boulevard, Pasadena, CA 91125, USA
[3] Department of Astrophysics, American Museum of Natural History, Central Park West at 79th Street, New York, NY 10024, USA
[4] Department of Astronomy and Astrophysics, University of California, Santa Cruz, CA, USA
[5] Planétarium de Montréal, Espace pour la Vie, 4801 Avenue Pierre-de Coubertin, Montréal, Québec, Canada
[6] Trottier Institute for Research on Exoplanets, Université de Montréal, Département de Physique, C.P. 6128 Succ. Centre-ville, Montréal, QC H3C 3J7, Canada
[7] Department of Physics, Astronomy and Mathematics, University of Hertfordshire, Hatfield, UK
[8] Department of Astronomy, University of Texas at Austin, Austin, TX, USA
[9] Department of Physics & Astronomy, Amherst College, Amherst, MA, USA
[10] School of Physics, Trinity College Dublin, The University of Dublin, Dublin 2, Ireland
[11] United States Naval Observatory, Flagstaff Station, 10391, West Naval Observatory Road, Flagstaff, AZ 86005, USA
[12] Department of Physics and Astronomy, San Francisco State University, 1600 Holloway Avenue, San Francisco, CA 94132, USA
[13] Department of Physics, Graduate Center, City University of New York, 365 5th Avenue, New York, NY 10016, USA
[14] Department of Physics and Astronomy, Hunter College, City University of New York, 695 Park Avenue, New York, NY, 10065, USA
[15] Backyard Worlds: Planet 9, USA
[16] Osservatorio Astronomico di Torino: Pino Torinese, Piemonte, IT, Italy
[17] Departamento de Astronomia, Universidad de Chile, Casilla 36-D, Santiago, Chile
Received 2025 September 8; revised 2025 November 21; accepted 2025 November 22; published 2026 January 2

Abstract

Studying cold brown dwarfs is key to understanding the diverse characteristics of cold giant exoplanets atmospheres. COCONUTS-2 is a wide binary system composed of a T9 brown dwarf and an M3 star, which presents a unique opportunity to characterize a cold benchmark brown dwarf. As part of a JWST program to study the range of physical and atmospheric properties of the coldest brown dwarfs, we obtained NIRSpec G395H spectra ($R \sim 2700$, $2.87-5.13\,\mu$m) and MIRI F1000W, F1280W, and F1800W photometry for COCONUTS-2 b. In this work, we find a 99% probability of the system belonging to the Corona of Ursa Major moving group (414 ± 23 Myr) using BANYAN Σ and its full kinematics. We also reestimate the astrometry of COCONUTS-2b using the MIRI data. We support this membership with a comparison of the rotation period, metallicity, and C/O ratio of the group with those of the COCONUTS-2 system. We also calculate its bolometric luminosity, which, combined with our age estimation, allows us to derive its mass, effective temperature, surface gravity, and radius with high precision. As a result of our analysis, we support the conclusion that COCONUTS-2 b is a planetary-mass object ($7.5 \pm 0.4\,M_{\rm Jup}$), which was likely formed via the same mechanism as stars. In addition we compare the JWST spectrum to another object in the sample, J082507.35+280548.5 (0825+2805), a Y0.5 brown dwarf, which is a candidate member of the same moving group, but has a lower mass ($3.7 \pm 0.2\,M_{\rm Jup}$). We identify absorption feature differences, which could indicate that 0825+2805 has stronger vertical mixing.

Unified Astronomy Thesaurus concepts: Low mass stars (2050); Brown dwarfs (185); T dwarfs (1679); Young star clusters (1833); Stellar ages (1581); Exoplanet atmospheres (487); Exoplanet formation (492)

1. Introduction

Brown dwarfs are objects with masses $< 78.5\,M_{\rm Jup}$ (G. Chabrier et al. 2023; with previous estimations such as 75 $M_{\rm Jup}$ from S. S. Kumar 1963; and 70 $M_{\rm Jup}$ from T. J. Dupuy & M. C. Liu 2017) that, unlike stars, do not burn hydrogen in their core. Although they are more massive than exoplanets, their cold atmospheres resemble these objects. Furthermore, brown dwarfs can be observed independently of a host star, making them the perfect laboratory to study exoplanet atmospheres. However, one of the main difficulties when studying brown dwarfs is the

luminosity–age–temperature degeneracy (e.g., A. Burrows et al. 1997). After formation, brown dwarfs cool with time, and go through different spectral types (e.g., D. Saumon & M. S. Marley 2008). For example, if we measure a cold effective temperature for an object (for example 1900 K), we cannot distinguish if this object is high mass and old (75 $M_{\rm Jup}$, $\sim$5 Gyr), or low mass and young (13 $M_{\rm Jup}$, $\sim$10 Myr). Studying atmospheric composition of brown dwarfs is even more complex, given that to the problem described above, we also add parameters such as the C/O ratio and the $K_{\rm zz}$ diffusion parameter (D. Saumon et al. 2012). Benchmark objects with known properties that reduce the degrees of freedom are key to refining models and ultimately fully understanding their atmospheres (D. J. Pinfield et al. 2006; M. C. Liu et al. 2008; M. W. Phillips et al. 2024). Brown dwarfs in a binary with a main-sequence star (e.g., J. R. Crepp et al. 2018;

E. L. Rickman et al. 2020; M. W. Phillips et al. 2024; A. Rothermich et al. 2024; J. W. Xuan et al. 2024), or that belong to moving groups (e.g., K. M. Aller et al. 2016; J. Gagné et al. 2023), are perfect benchmark candidates given that we can use the primary, or group members, to estimate properties of the brown dwarf such as metallicity and age.

In this work we study COCONUTS-2 b, or WISEP J075108.79-763449.6 (J. D. Kirkpatrick et al. 2011), a cold (430 K; Z. Zhang et al. 2021a) brown dwarf, which was one of the 12 objects observed as part of the JWST GO 2124 program from Cycle 1 (PI: J. Faherty). This program has the goal of explaining the spread in the Spitzer IRAC color–magnitude diagram of cold brown dwarfs, spanning $1-2$ absolute [4.5] magnitudes. The study presented here is part of a series of publications resulting from the data of the JWST GO 2124 program that include: the identification and analysis of methane emission on CWISEP J193518.59−154620.3 (J. K. Faherty et al. 2024; G. Suárez et al. 2025), a study of the full SED of 2MASS J04151954−0935066 (S. Alejandro Merchan et al. 2025), the analysis and identification of blended binaries (D. C. Bardalez Gagliuffi et al. 2025; M. De Furio et al. 2025), individual retrieval analysis (M. Rowland et al. 2025, in preparation; J. Copeland et al. 2025, in preparation), sample papers doing forward modeling (B. Lacy et al. 2025, in preparation), retrieval analysis (B. Burningham et al. 2025, in preparation), and an analysis of the spectral sequence (J. K. Faherty et al. 2025, in preparation). COCONUTS-2 b is particularly interesting given that it is in a wide binary system with an M3 type star, separated by 6471 au (Z. Zhang et al. 2021a). Furthermore, COCONUTS-2 is a potential member of the young moving group Corona of Ursa Major (CUMA; F. Marocco et al. 2024), making the system ideal to study the properties of cold brown dwarfs anchored on the properties of the primary and the group. COCONUTS-2 b is also an underluminous object in the Spitzer color–magnitude diagram, and also exhibits K-band flux suppression characteristic of T subdwarfs, as seen in a low signal-to-noise ratio (SNR) spectrum (J. D. Kirkpatrick et al. 2011, 2021), making it a compelling target for JWST spectroscopic follow-up. The JWST GO 2124 program collected spectra and photometry to constrain key physical properties, including age, metallicity, clouds, C/O ratio, vertical mixing, chemical disequilibrium, elemental abundances, and binarity. This type of analysis has been extensively applied to warmer objects such as L and early T dwarfs (A. J. Burgasser et al. 2010; J. K. Faherty et al. 2012, 2016), but remains scarce for late T and Y dwarfs (Z. Zhang et al. 2021b).

The goal of this work is to study the properties of the COCONUTS-2 system in the context of the moving group to which it has been tentatively linked. In Section 2 we describe the JWST spectrum and photometry we obtained in Cycle 1, as well as the compilation of data available in the literature. In Section 3 we analyze the membership of COCONUTS-2 to the CUMA, which we use to establish the age of the system. We also use the members of CUMA and all the information compiled on the COCONUTS-2 system to comment on its formation mechanism. In Section 4 we combine all the available data to estimate the bolometric luminosity of both components of the system, and estimate the mass, radius, effective temperature, and surface gravity, assuming the age of CUMA. In Section 5 we present a detailed analysis of the molecules found in the atmosphere of COCONUTS-2 b by comparing the JWST spectrum to molecular opacity cross sections, and a forward-modeling analysis of all the available spectra for this object. In addition, we compare

COCONUTS-2 b to a second object from the JWST GO 2124 program, J082507.35+280548.5, which has high probability of belonging to the same cluster. Finally in Section 6 we include the conclusions of this work.

2. Data

As part of JWST GO 2124 program, we collected near-infrared spectra with the highest attainable resolution ($R \sim 2700$), and mid-infrared photometry of COCONUTS-2 b. In this section we describe the new data, and the compilation of available data from the literature for both components of the system.

2.1. Spectra

In this section we describe the spectra available for COCONUTS-2b, both from the literature and the JWST GO 2124 program.

2.1.1. JWST/NIRSpec Spectrum

As part of JWST Cycle 1, we obtained a spectrum of COCONUTS-2 b using the JWST Near Infrared Spectrograph (NIRSpec; P. Jakobsen et al. 2022) G395H disperser, which provides the highest resolution spectrum attainable (average $R \sim 2700$) in the wavelength range $2.87-5.13~\mu$m.[18] We show the JWST spectrum of COCONUTS-2 b in Figure 1. In this work, we used the data generated using the calibration software version 1.17.1, and the file that was made on 2025 March 19. This spectrum has a median SNR of 16 in the full wavelength range, or 30 in the range $>3.79~\mu$m.

2.1.2. Gemini/FLAMINGOS-2 Spectrum

In addition, we included in our analysis a Gemini-South FLAMINGOS-2 spectrograph (S. Eikenberry et al. 2004, 2008) spectrum ($0.94-2.46~\mu$m) of COCONUTS-2 b published by Z. Zhang et al. (2025). We downloaded the raw data together with the calibration files from the Gemini archive,[19] and we rereduced the data using `PypeIt`[20] (J. X. Prochaska et al. 2020a, 2020b, 2020c). The spectrum was taken in two wavelength ranges: JH band ($0.94-1.96~\mu$m), and K band ($1.96-2.46~\mu$m). We decided to rereduce only the JH band, and include only the available photometry for the K band (see Section 2.2). Using the photometry, we estimated that the K band contributes approximately 2% of the bolometric flux. In addition, the SNR of the K band is low (SNR ≈ 2; Z. Zhang et al. 2025). Therefore, we concluded that the photometry in the K band provides a good approximation of the flux. Following the description on Z. Zhang et al. (2025), we used the standard HIP 43762 to perform flux calibration, we used the ABBA pattern to remove the background contamination, and we performed a telluric correction using the standard star. As a result we obtained a spectrum with an average resolution of $R \sim 900$ in the wavelength range $0.94-1.96~\mu$m, with SNR ≈ 8. We found that our reduction is consistent with the result from Z. Zhang et al. (2025). We included a detailed discussion on the comparison of the two spectra in the Appendix.

---

[18] The specific observations analyzed can be accessed via DOI: 10.17909/rxm9-qd05.

[19] https://archive.gemini.edu/searchform

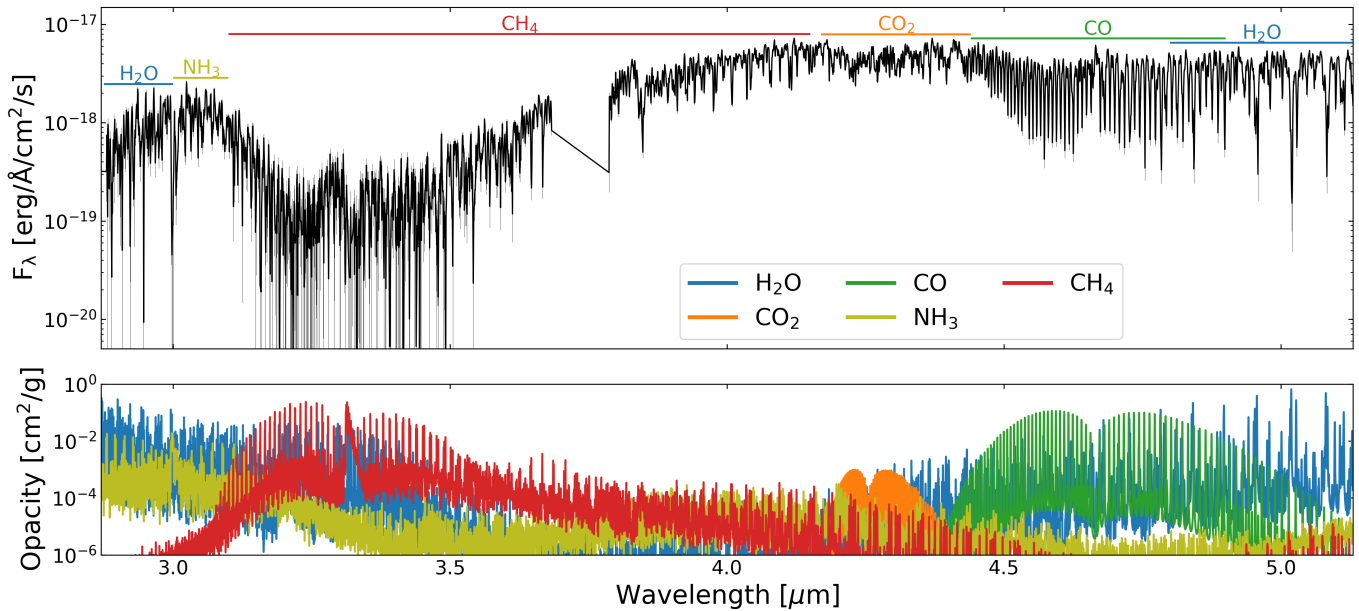[20] https://pypeit.readthedocs.io/en/1.17.1/index.html

Figure 1. Top panel shows the JWST spectrum of COCONUTS-2 b in the filter G395H with horizontal lines indicating the molecular features which are recognizable in the spectrum. We also included the uncertainty in the flux in light gray. Bottom panel shows the opacities for each identified molecule which we obtained from the DACE database (R. J. Barber et al. 2006; L. S. Rothman et al. 2010; S. N. Yurchenko et al. 2011; A. A. A. Azzam et al. 2016; R. J. Hargreaves et al. 2020; S. L. Grimm et al. 2021; J. Tennyson et al. 2024). See Section 5 for a detailed description and discussion.

2.2. Photometry

In this section we decribe the photometry available for the COCONUTS-2 system, both from the literature and the JWST GO 2124 program.

2.2.1. COCONUTS-2 A

COCONUTS-2 A is a bright nearby M dwarf, which was observed by several surveys, therefore we were able to compile photometry points covering almost the full spectral energy distribution (SED; $0.15-22.09$ μm) from the NASA/ IPAC Infrared Science Archive (IRSA).[21] We show the compiled data in Table 1.

2.2.2. COCONUTS-2 b

We compiled the existing photometry in the literature for COCONUTS-2 b, which we show in Table 1. In addition, as part of JWST Cycle 1 we obtained three photometry points using the Mid-Infrared Instrument (MIRI) in the bands F1000W ($8.8-11.1$ μm), F1280W ($11.3-14.3$ μm), and F1800W ($16.0-20.3$ μm).[22] For our analysis, we used the data which were generated using the calibration software version 1.17.1, and the files were created on 2025 March 19. For each of the three bands we used the photometry which was calculated using a 70% encircled energy circular aperture in the Vega system by the JWST pipeline (D. Dicken et al. 2024). These three points can be found in Table 1.

Using the new JWST spectrum in Figure 1, we estimated synthetic photometry for COCONUTS-2 b, and obtained W1 = 17.60 ± 0.12 mag, W2 = 14.52 ± 0.03, [3.6] = 16.97 ± 0.12, and [4.5] = 14.59 ± 0.03. To account for the flux in the gap of the JWST spectrum in the wavelength range [3.68,

3.79] μm, we applied a simple linear interpolation. When we compared the synthetic photometry to the values in the literature (Table 1), we found that while [4.5] and W2 are consistent, the synthetic values for [3.6] and W1 are 0.5 mag fainter than the literature values. These differences are consistent with the results from S. A. Beiler et al. (2024), who compared synthetic photometry from low-resolution JWST spectra to the literature value of a sample of 23 late-type T and Y dwarfs. They found a median scatter of 0.3 mag in W1, which they note is consistent with the preflight uncertainty goal of $\sim$10%, and a systematic difference in the [3.6] band of around 0.3 mag. As S. A. Beiler et al. (2024) found these differences across a large population of objects, it suggests that is not related to variability. The same conclusion was reached by K. L. Luhman et al. (2024), who also suggested that the differences could be due to errors in the filter response.

To study the variability hypothesis, we downloaded the photometry (and corresponding epoch) available on IRSA for COCONUTS-2 b in the W1 and W2 bands from the WISE (E. L. Wright et al. 2010), AllWISE (R. M. Cutri et al. 2013; F. Marocco et al. 2021); and NEOWISE (A. Mainzer et al. 2011) catalogs. In total we collected photometry spanning more than 13 yr, with a cadence of 6 months. We did not find significant trends of long-term variability for W1. Using the NEOWISE data—given they have more photometry points— we estimated a reduced χ-squared value of 1.59 ($\nu = 154$) when compared to the average photometry, which clearly shows no variability. In the case of W2, we did not find variability either (reduced χ-squared of 0.83 ($\nu = 275$) for the NEOWISE data), but in this case all the data agree well with the synthetic photometry.

2.3. Astrometry

Astrometry for COCONUTS-2 A is provided by Gaia (Gaia Collaboration et al. 2023b), while astrometry for COCONUTS-

Table 1
Properties of COCONUTS-2

	COCONUTS-2 A	References	COCONUTS-2 b	References
Photometry				
GALEX/GALEX FUV [mag]	17.704 ± 0.161	Bianchi2011	⋯	⋯
GALEX/GALEX NUV [mag]	16.459 ± 0.065	Bianchi2011	⋯	⋯
SLOAN/Sloan Digital Sky Survey (SDSS) u [mag]	13.474 ± 0.057	Ahumada2022	⋯	⋯
TYCHO/TYCHO B [mag]	13.424 ± 0.313	Hog2000	⋯	⋯
SLOAN/SDSS g [mag]	12.155 ± 0.067	Ahumada2022	⋯	⋯
G_{BP} (Gaia/Gaia3 G_{BP}) [mag]	11.558 ± 0.055	Gaia2023	⋯	⋯
TYCHO/TYCHO V [mag]	11.636 ± 0.119	Hog2000	⋯	⋯
G (Gaia/Gaia3 G) [mag]	10.162 ± 0.054	Gaia2023	⋯	⋯
SLOAN/SDSS r [mag]	10.541 ± 0.078	Ahumada2022	⋯	⋯
SLOAN/SDSS i [mag]	9.075 ± 0.079	Ahumada2022	⋯	⋯
G_{RP} (Gaia/Gaia3 G_{RP}) [mag]	8.995 ± 0.055	Gaia2023	⋯	⋯
SLOAN/SDSS z [mag]	8.600 ± 0.090	Ahumada2022	⋯	⋯
Gemini/FLAMINGOS-2 Y [mag]	⋯	⋯	20.020 ± 0.100	Leggett2015
J_{2MASS} (Two Micron All Sky Survey (2MASS)/2MASS J) [mag]	7.417 ± 0.057	Skrutskie2006	⋯	⋯
J_{MKO} (NSFCam J) [mag]	⋯	⋯	19.340 ± 0.050	Kirkpatrick2011
H_{MKO} (NSFCam H) [mag]	⋯	⋯	19.680 ± 0.130	Leggett2015
H_{2MASS} (2MASS/2MASS H) [mag]	6.835 ± 0.061	Skrutskie2006	⋯	⋯
Ks_{2MASS} (2MASS/2MASS Ks) [mag]	6.563 ± 0.058	Skrutskie2006	⋯	⋯
K_{MKO} (NSFCam K) [mag]	⋯	⋯	20.030 ± 0.200	Leggett2015
W1 (Wide-field Infrared Survey Explorer (WISE) W1) [mag]	6.477 ± 0.071	Marocco2021	17.080 ± 0.036	Marocco2021
[3.6] (IRAC I1) [mag]	⋯	⋯	16.432 ± 0.036	Kirkpatrick2011
[4.5] (IRAC I2) [mag]	⋯	⋯	14.621 ± 0.020	Kirkpatrick2011
W2 (WISE W2) [mag]	6.287 ± 0.058	Marocco2021	14.610 ± 0.015	Marocco2021
AKARI/IRC S9W [mag]	6.036 ± 0.069	Ishihara2010	⋯	⋯
MIRI F1000W [mag]	⋯	⋯	12.910 ± 0.005	This work
IRAS/IRAS 12mu [mag]	6.147 ± 0.121	Abrahamyan2015	⋯	⋯
W3 (WISE W3) [mag]	6.311 ± 0.056	Cutri2021	11.911 ± 0.155	Cutri2021
MIRI F1280W [mag]	⋯	⋯	12.386 ± 0.005	This work
MIRI F1800W [mag]	⋯	⋯	12.066 ± 0.010	This work
W4 (WISE/WISE W4) [mag]	6.077 ± 0.063	Cutri2021	⋯	⋯
Astrometry and kinematics				
Epoch [yr]	2016	Gaia2023	2025	This work
R.A. [deg]	117.30085	Gaia2023	117.78671	This work
Decl. [deg]	−76.70272	Gaia2023	−76.5804	This work
PM R.A. [mas yr^{-1}]	-102.15 ± 0.02	Gaia2023	-104.80 ± 2.80	This work
PM Decl. [mas yr^{-1}]	-192.92 ± 0.02	Gaia2023	-189.70 ± 4.50	This work
Parallax [mas]	91.83 ± 0.02	Gaia2023	97.90 ± 3.70	This work
Radial velocity [km s^{-1}]	1.19 ± 0.61	Gaia2023	0.10 ± 4.50	Faherty2025
Physical properties				
Age [Myr]	414 ± 23	This work	414 ± 23	This work
L_{bol} [erg s^{-1}]	$(7.31 \pm 0.12) \times 10^{31}$	This work	$(2.73 \pm 0.22) \times 10^{27}$	This work
$\log L_{bol}/L_{\odot}$	-1.719 ± 0.007	This work	-6.15 ± 0.03	This work
Mass [$M_{\odot}$, M_{Jup}]	$0.40^{+0.01}_{-0.02}$	This work	$7.50^{+0.40}_{-0.40}$	This work
Radius [$R_{\odot}$, R_{Jup}]	$0.366^{+0.005}_{-0.014}$	This work	$1.122^{+0.005}_{-0.004}$	This work
$\log g$ [dex]	$4.91^{+0.02}_{-0.01}$	This work	$4.17^{+0.02}_{-0.02}$	This work
T_{eff} [K]	3552^{+65}_{-32}	This work	493^{+9}_{-9}	This work

References. Abrahamyan2015: H. V. Abrahamyan et al. (2015); Ahumada2022: R. Ahumada et al. (2022); Bianchi2011: L. Bianchi et al. (2011); Cutri2021: R. M. Cutri et al. (2021); Faherty2025: J. K. Faherty (2025, in preparation); Gaia2023: Gaia Collaboration et al. (2023a); Hog2000: E. Høg et al. (2000); Ishihara2010: D. Ishihara et al. (2010); Kirkpatrick2011: J. D. Kirkpatrick et al. (2011); Kirkpatrick2021: J. D. Kirkpatrick et al. (2021); Leggett2015: S. K. Leggett et al. (2015); Marocco2021: F. Marocco et al. (2021); and Skrutskie2006: M. F. Skrutskie et al. (2006).

2 b is available from J. D. Kirkpatrick et al. (2021). The J. D. Kirkpatrick et al. (2021) values are based on dedicated New Technology *Telescope, Softt (*NTT/SofI) observations (R. L. Smart et al. 2013) covering a baseline of ∼5.3 yr. Several new NTT/SofI observations have been acquired as part of the NPARSEC program (R. L. Smart et al. 2013) since J. D. Kirkpatrick et al. (2021), and with the addition of the JWST/MIRI images presented here we derived updated parallax and proper motion (PM) for COCONUT-2 b with data now spanning a baseline of nearly 12 yr.

The observing strategy and data reduction for the NTT/SofI data followed the procedure described in detail in R. L. Smart et al. ([2013](#)). We refined the astrometric calibration of the SofI data by finding Gaia sources in the images and fitting a transformation between their NTT and Gaia Data Release 3 (DR3) coordinates.

First, we detected and measured the centroid for all sources in each image using `imcore`.[23] The x- and y-pixel coordinates measured by `imcore` are converted to α and δ (R.A. and decl.) using each image's world coordinates system, and then matched to Gaia DR3 using a $3''$ matching radius. We found between $\sim$60 and $\sim$80 Gaia sources in each NTT image. The positions of matching Gaia sources are propagated from the Gaia epoch (2016.0) to the epoch of each observation using their measured parallax and proper motion. We then derived a transformation between our measured coordinates and the Gaia coordinates by projecting both onto a tangent plane whose tangent point is defined by the CRVAL1 and CRVAL2 FITS header keywords. Finally, we fit for a six-parameter transformation, which accounts for offsets, rotation, skew, and scaling. The parameters of the transformation were determined using the IDL routine `mpfit` (C. B. Markwardt [2009](#)).[24] The residuals of the fit are added in quadrature to the measurement errors to compute the final coordinate uncertainties.

Astrometric distortion was accounted for by deriving a distortion map. To do that, we took the postcalibration astrometric residuals (i.e., $\Delta\alpha = \alpha_{\rm Gaia} - \alpha_{\rm NTT}$ and $\Delta\delta = \delta_{\rm Gaia} - \delta_{\rm NTT}$) for all stars from all NTT images, and produced a map of residuals as a function of position on the detector. We binned this map using an $N \times N$ grid, and in each bin we determined the median residuals. We corrected the position of our target in each image by adding the $\Delta\alpha$ and $\Delta\delta$ values for the appropriate bin.

JWST/MIRI data were calibrated following the same procedure, with two important differences. First, because we have few reference stars, we could only fit for a three-parameter transformation, which accounts only for offset and rotation. Second, we did not need to derive a distortion map, since MIRI images are distortion corrected by the imaging pipeline (see, e.g., Section 7 in D. Dicken et al. [2024](#)).

We then combined the JWST and NTT measurements and fit for parallax and PM following the procedure described in J. D. Kirkpatrick et al. ([2019](#), [2021](#)). The results are presented in Table [1](#). The new values are consistent within 1σ with those presented in J. D. Kirkpatrick et al. ([2021](#)).

3. Age Estimation

Being a binary, COCONUTS-2 presents a valuable opportunity to break the luminosity–age–temperature degeneracy of brown dwarfs. In this work we present full kinematics for both components of the binary. F. Marocco et al. ([2024](#)) noted the potential membership of COCONUTS-2 to the CUMA moving group, which has the same age as the Ursa Major (UMA) group, the core of CUMA: $414 \pm 23\,$Myr (J. Jones et al. [2015](#)). In this section, we describe how we confirmed that membership using the 3D kinematics of both objects, rotation period, metallicity, and C/O ratio.

As shown in Table [1](#), COCONUTS-2 A was observed by Gaia DR3, which provided precise 3D kinematics and position.

In the case of COCONUTS-2 b, the radial velocity was estimated by J. K. Faherty et al. (2025, in preparation)—another work in the series of the JWST GO 2124 program—and in this work we remeasured the astrometry using the MIRI photometry (see Section [2.3](#)). In short, for the calculation of radial velocity J. K. Faherty et al. (2025, in preparation) split the spectrum in windows that slightly overlap with each other, and in each window they built a forward model combining the Sonora Diamondback atmosphere models (C. V. Morley et al. [2024](#)), a Gaussian line-spread function (with its width determined by only one parameter), a Doppler shift (one parameter), and a linear blaze function (two parameters). Then they run a Markov Chain Monte Carlo (MCMC) to sample the parameter space and pick the best-fitting model. After the fit, they checked if the residuals were representative of the expected errors. If they were not, they identified what error inflation would make the residuals follow a normal distribution with 1σ deviation ($\chi^2 = 1$). Then they rerun the MCMC fit with this error inflation term in the spectrum. This extra step of inflating the uncertainties allows one to get more representative errors when the model is a poor fit to the data. After the fit, they inspected the radial velocity measurements as a function of wavelength and checked that there were no significant trends. Finally, they averaged the measurements to obtain the final radial velocity and uncertainty.

Taking advantage of the 3D kinematics and 3D positions of both components of COCONUTS-2, we used BANYAN Σ (J. Gagné et al. [2018](#)) to estimate the membership of the binary. BANYAN Σ uses Bayesian inference to estimate the probability of an object belonging to a known association within 300 pc. This probability is calculated by comparing the 3D position and kinematics of the object to the position and velocity models of each group. Using BANYAN Σ, we estimated a 99% probability for each of the components of belonging to the CUMA group. Because two of the parameters of COCONUTS-2 b—radial velocity and parallax—exhibit large uncertainties, we performed a statistical test of the membership probability. We simulated 1000 stars with a random radial velocity measurement drawn a normal distribution defined by the value and uncertainty of the radial velocity measurement for COCONUTS-2 b. The rest of the parameters were left unmodified. We used Banyan Σ to calculate the probability of membership of each of these 1000 stars, and obtained a 99% probability of belonging to CUMA for all the iterations. We repeated this processes but this time the random parameter was the parallax, and obtained the same result, confirming the robustness of the result.

To further confirm the membership of COCONUTS-2 to CUMA, we study the chance alignment probability, rotation period distribution, metallicity, and C/O ratio of the group. We describe each of these checks below. We obtained the members of CUMA from the Montreal Open Clusters and Associations (MOCA) database[25] (J. Gagné [2024](#); J. Gagné et al. 2025, in preparation). Besides the membership according to kinematics, the stars in MOCA are classified as confirmed, high-likelihood, and candidate members of clusters or young associations, depending on if extra information is available, such as magnetic activity and rotation periods, which supports that they are young. In Figure [2](#) we show the 1782 members of CUMA: 1669 candidate members shown in light-purple and

---

[23] http://casu.ast.cam.ac.uk/surveys-projects/software-release/imcore
[24] http://cow.physics.wisc.edu/~craigm/idl/fitting.html
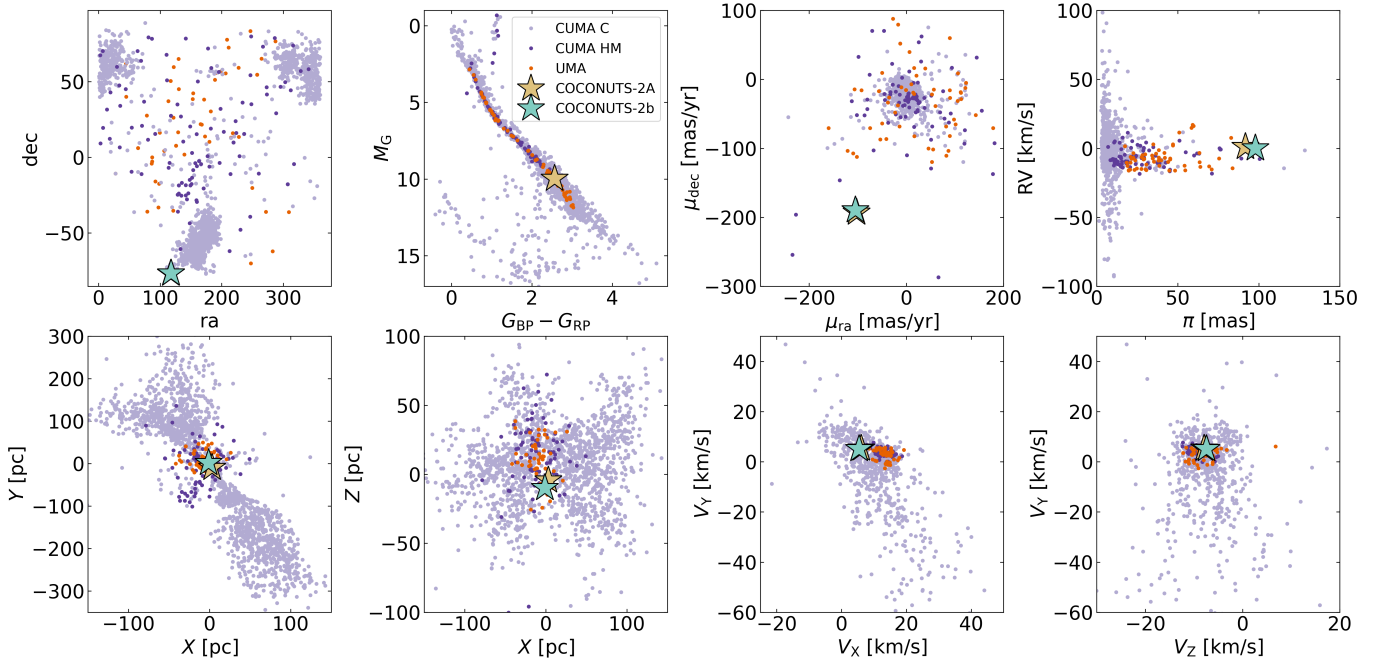
[25] https://mocadb.ca/

Figure 2. Astrometric and photometric plots for the members of CUMA. The top row shows R.A., decl., the Gaia color–magnitude diagram, PM R.A. ($\mu_{R.A.}$), PM decl. ($\mu_{decl.}$), radial velocity, and parallax (π). The bottom row shows the 3D Galactic positions (X, Y, Z) and the 3D Galactic velocities (V_X, V_Y, V_Z). We show in light-purple the candidate members ("CUMA C") and in purple the high-likelihood members ("CUMA HM"). We obtained these classifications from the MOCA database. We also include in orange the members of the UMA cluster from B. K. Capistrant et al. (2024). In a yellow star we show COCONUTS-2 A, and in green COCONUTS-2 b. We find that the components of COCONUTS-2 agree well with the cluster in 3D velocity and position, while staying closer to each other, confirming that they are a binary.

113 high-likelihood members in purple. We also included the 56 targets identified as members of the UMA cluster—the core of CUMA—by B. K. Capistrant et al. (2024) in orange. We found that 26 of these objects were also included in our list of CUMA members. The two star symbols of Figure 2 represent the two members of the COCONUTS-2 system. The 3D positions and velocities of the two objects agree well with the members of the cluster. In addition, the two components have similar positions and velocities, supporting that these two objects are in a binary, which agrees with previous results (Z. Zhang et al. 2021a).

3.1. Kinematics Chance Alignment

The members of the CUMA group have a large spread both in position and velocity, as can be seen in Figure 2. Therefore chance association with the group is a possibility. Banyan Σ includes a complex description of what a field star looks like, and compares it to models of the groups included. However, by default its priors are set up such that every association has a recovery rate of ∼90% when using a probability of 90% threshold, with input uncertainties typical of Gaia. There are documented probability to false-positive rate mappings for each of the published associations, but this is not the case of CUMA. Therefore we decided to do a Monte Carlo test as a first characterization of the expected false-positive rate in CUMA. To test how likely it is to identify a field star as a member of CUMA we selected 4000 random stars from the 150 pc sample from Gaia DR3 with radial velocities, and randomized the R.A. values, decl. values, parallaxes, and the uncertainties, but left the combination of PM R.A., PM decl., and radial velocities untouched. For our test we replaced the radial velocities uncertainty, and tried seven cases: 1%, 10%,

20%, 30%, 40%, 50%, and 60% uncertainty. With a 50% uncertainty in the radial velocity, which is close to the 45% uncertainty of COCONUTS-2 b (see Table 1), we found that one in every 91 stars got randomly assigned a membership to CUMA with a probability larger than 95%, which represents a 1.1% chance of alignment (1.7% with a cut at 90%). We found that this probability decreases to 0.68% for an uncertainty of 10%, and 0.65% with 1% uncertainty. This analysis shows that, even using only kinematics, the probability of a random assignment of membership to CUMA is small, but the contamination needs to be taken into account.

3.2. Rotation Periods

As an additional test to confirm the membership of COCONUTS-2 to the CUMA group, we used rotation periods. COCONUTS-2 A has a measured rotation period of 2.83 ± 0.28 days (Z. Zhang et al. 2021a), which we compared to the rest of the members of the cluster. We measured rotation periods for all the members of the group using the data from the Transiting Exoplanet Survey Satellite (TESS; G. R. Ricker et al. 2015). We analyzed a sample of 690 members of CUMA, which are classified as candidates or high-likelihood members, and which are brighter than $G < 15$ mag and have $(G_{BP} - G_{RP}) > 0.5$. We decided on this magnitude cut given that we found that 80% of stars fainter than 15 mag exhibited flat light curves. For the light-curve extraction, we followed the procedure described in M. Popinchalk et al. (2023), which we briefly summarize below.

We used Tesscut (C. E. Brasseur et al. 2019) to download TESS full-frame image cutouts of 40 × 40 pixels size, and extracted the light curves from them. We detrended the light curves using two methods. The first is the causal pixel

Table 2
Description of the Columns in the Sample of Members of CUMA with
Rotation Periods and Metallicity Measurements

Column[a]	Column Description
moca_oid	ID internal to the MOCA database
designation	Normal designation of the target
bp_rp	Gaia ($G_{BP} - G_{RP}$) color
period	Rotation period (days)
m_h	[M/H]
m_h_error	[M/H] uncertainty
m_h_ref	[M/H] reference
fe_h	[Fe/H]
fe_h_error	[Fe/H] uncertainty
fe_h_ref	[Fe/H] reference
c_fe	[C/Fe]
c_fe_error	[C/Fe] uncertainty
c_fe_ref	[C/Fe] reference
o_fe	[O/Fe]
o_fe_error	[O/Fe] uncertainty
o_fe_ref	[O/Fe] reference
ya_prob	Probability of belonging to a young association

Note.
[a] Full table is available online.

model (CPM), which we implemented using the package `unpopular` (S. Hattori et al. 2022). CPM is based on the idea that variations in brightness which are shared by several pixels are TESS systematics. The package `unpopular` models these variations by selecting neighboring stars around the target of interest and subtracting their combined signal from the target's light curve. This method is particularly useful when the star is faint. The second method we used is simple aperture photometry around the target. This method consists of extracting the light curve using a 4 pixel circular aperture, which works best for bright stars where TESS systematics is less important (J. L. Curtis et al. 2019; M. Popinchalk et al. 2023). In order to apply these methods and inspect each light curve, we used the package `Tess_check` (J. L. Curtis et al. 2019).

After extracting the light curves, we used `LombScargle` from the package `astropy` to measure the rotation period of each star. The resulting rotation period measurements are in Table 2 and are shown in Figure 3 in light-purple circles. We removed stars with RUWE > 1.4 from the figure, to discard possible binaries (C. Fabricius et al. 2021). In addition, we included the rotation period measurements for the UMA cluster from B. K. Capistrant et al. (2024) in orange, and several known clusters color coded by age (J. L. Curtis et al. 2020). The yellow five-point star in the figure represents the rotation period and color of COCONUTS-2 A. We found that the sequence of rotation periods of CUMA agrees with the sequence of UMA, which supports that they have the same age. In addition, COCONUTS-2 A agrees well with the locus of the CUMA group in the rotation versus color plot, supporting its membership to the group.

Using the rotation periods of the members of CUMA and UMA, we estimated the age of the two clusters with `ChronoFlow` (P. R. Van-Lane et al. 2025). `ChronoFlow` models the evolution of stellar rotation periods as a function of ($G_{BP} - G_{RP}$) color using a neural-network-based probabilistic framework known as a conditional normalizing flow. This

particular model is flexible to deal with complex density distributions, which was trained on a sample of known clusters with rotation period measurements. We obtained an age of 609^{+354}_{-276} Myr for CUMA and 549^{+191}_{-230} Myr for the UMA cluster, which further support that both groups have the same age. In addition, the ages of both clusters are consistent with the previous age estimation for UMA (414 ± 23 Myr), which was calculated using stellar evolution models of a sample of A stars that belong to the cluster (J. Jones et al. 2015). We decided to continue using the previous age estimation given that the uncertainty is smaller.

3.3. Metallicity

As another method to test the membership of COCONUTS-2 to CUMA, we compared the metallicity of the primary and secondary to the members of the cluster. COCONUTS-2 A has a measured metallicity of [Fe/H] = 0.0 ± 0.08 dex from S. Hojjatpanah et al. (2019), and -0.05 ± 0.17 dex from Z. Zhang et al. (2021a). These measurements were made using high-resolution spectra and the ($V - K$)–metallicity relation, respectively. We opted for the former, as it is more precise. COCONUTS-2 b has an estimated metallicity from Z. Zhang et al. (2025) who found subsolar atmospheric [M/H] in the range $[-0.395, 0.024]$ dex, by fitting the Gemini/FLAMINGOS-2 spectrum with different atmospheric models. In this work, we performed a forward-modeling analysis of both the Gemini/FLAMINGOS-2 spectrum and the JWST spectrum together, and we found that without any constrains on the fit, we obtained [M/H] = $-0.337^{+0.016}_{-0.046}$ dex, which is consistent with the results from Z. Zhang et al. (2025). For a detailed description of this analysis, see Section 5.2.

To obtain metallicity measurements for the members of CUMA, we crossmatched the sample with APOGEE DR17 (Abdurro'uf et al. 2022), GALAH DR3 (S. Buder et al. 2021), RAVE Data Release 6 (DR6; M. Steinmetz et al. 2020), and LAMOST Data Release 7 (DR7; Y. Luo et al. 2019). Comparisons of metallicity measurements for stars common to these catalogs indicate that they are consistent (R. Carrera et al. 2019; V. Hegedűs et al. 2023). For each of the three catalogs we did a positional crossmatch using a 3″ radius with the Tool for Operations on Catalogues and Tables (M. B. Taylor 2005). Applying the corresponding quality flags from each catalog to select the best abundance measurements, we obtained 62 measurements of [Fe/H] and 46 of [M/H]. The results for [Fe/H] and [M/H] together with the metallicities of COCONUTS-2 A and COCONUTS-2 b are shown in Figure 4, and compiled in Table 2. We also included in a black line the median value of [Fe/H] for the UMA cluster measured by A. M. Boesgaard et al. (1988): [Fe/H] = -0.079 ± 0.053 dex. This value was measured from high-resolution spectra of the members of the group. The median value of [Fe/H] for the UMA cluster agrees well with the distribution of CUMA members. The uncertainty in the measurement from A. M. Boesgaard et al. (1988) corresponds to the dispersion in [Fe/H] values of the individual members, and shows a smaller scatter than CUMA. Below we discuss this point further. The value of [Fe/H] of COCONUTS-2 A is well centered in the distribution of the CUMA members, which supports the membership of the system to the group. The value of [M/H] of COCONUTS-2 b is moderately subsolar, however it agrees with the distribution of the cluster within the uncertainty. One possible explanation for this
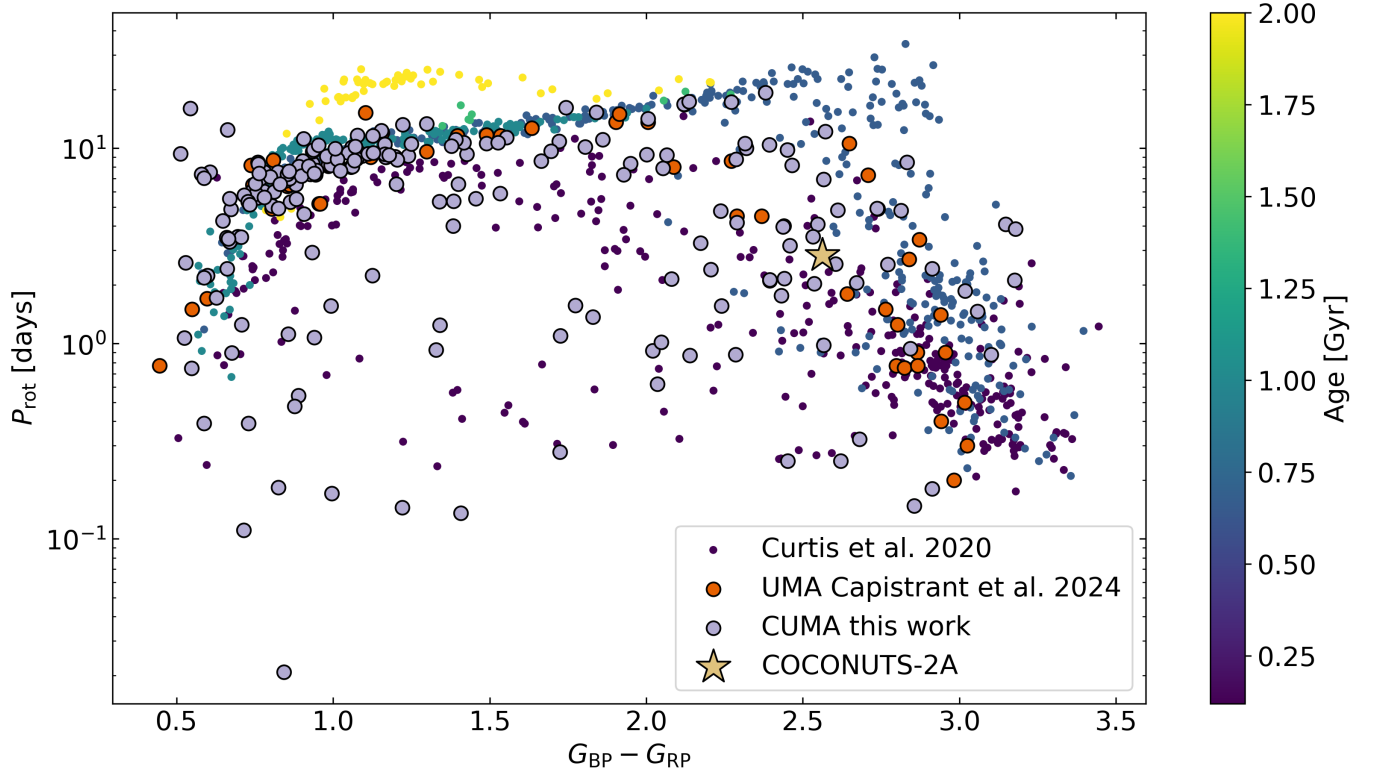
Figure 3. Rotation period in days as a function of the Gaia ($G_{BP} - G_{RP}$) color for CUMA. The candidates and high-likelihood members are shown in light-purple points. We included the members of the UMA cluster from B. K. Capistrant et al. (2024) in orange. In addition we show extra known young clusters with measured rotation periods, color coded by age. We included the clusters compiled by J. L. Curtis et al. (2020): Pleiades (120 Myr; L. M. Rebull et al. 2016), Praesepe (670 Myr; S. T. Douglas et al. 2017, 2019), NGC 6811 (1 Gyr; J. L. Curtis et al. 2019), NGC 752 (1.4 Gyr; M. A. Agüeros et al. 2018), NGC 6819 (2.5 Gyr; S. Meibom et al. 2015), and Ruprecht 147 (2.7 Gyr; J. L. Curtis et al. 2020). We also included COCONUTS-2 A as a yellow five-point star, which has a measured rotation period. We found that the members of CUMA agree with the rotation period sequence of UMA, confirming that the two groups have the same age. We also found that the rotation period of COCONUTS-2 A agrees with the locus of the CUMA group, providing further support for its membership in the group.

Figure 4. [Fe/H] and [M/H] measurements for the candidate members of CUMA collected from the APOGEE DR17, GALAH DR3, RAVE DR6, and LAMOST DR7 catalogs. We included in a black horizontal line, the value of [Fe/H] for the UMA cluster (A. M. Boesgaard et al. 1988). We also included as a vertical line, the value of [Fe/H] for COCONUTS-2 A and [M/H] for COCONUTS-2 b (See Section 5.2). The dotted vertical lines show the uncertainty in these two values. These measurements agree with the distribution of the moving group within the uncertainty, supporting the membership of COCONUTS-2 to the group.

difference is that there is a systematic uncertainty in the forward-modeling analysis which has not been calibrated yet. We plan to explore this scenario in future studies.

We found 10 candidate members of CUMA with a metallicity significantly different from the rest of the group (eight with [M/H] < −0.5 and two with [Fe/H] < −0.5). We found that these outliers have a large uncertainty and/or are stars with lower probability of belonging to CUMA, meaning that they have the largest difference in position and velocity from the center of the cluster. Therefore, these objects are loosely bound or not members. In order to study the intrinsic scatter of the distribution of metallicities, we made Figure 5. This figure shows in the left panel the metallicity as a function of the probability of each candidate member to belong to the moving group, and in the right panel the histogram of the metallicity values. Removing the extreme outliers, we estimated the median and the standard deviation of the [Fe/H] distribution for CUMA members, and we found −0.06 ± 0.25 dex, which agrees well with the value for the UMA cluster with a significantly larger scatter. We found that the large scatter is in part due to the uncertainty in the measurements of metallicity from the different catalogs. We calculated the median uncertainty of the available measurements in our sample for each catalog, and found values of, in increasing order, APOGEE DR17: 0.006 dex, LAMOST DR7:
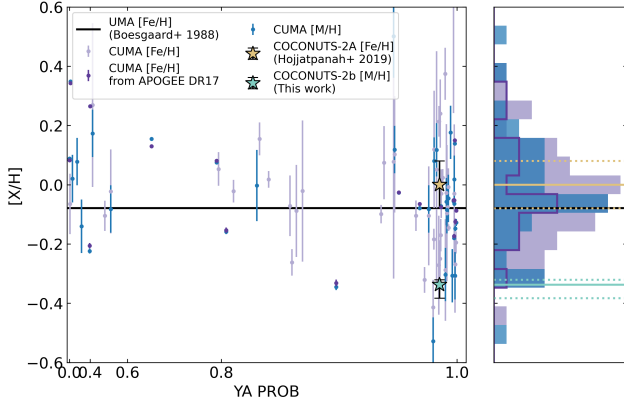
Figure 5. [Fe/H] and [M/H] measurements for the candidate members of CUMA collected from the APOGEE DR17, GALAH DR3, RAVE DR6, and LAMOST DR7 catalogs. In the left panel we show the metallicity as a function of the probability of belonging to the CUMA group, and in the right panel is the distribution of values. We included the value of [Fe/H] for COCONUTS-2 A and [M/H] for COCONUTS-2 b as five-point stars in the left panel and as horizontal lines in the right panel. The dotted horizontal lines show the uncertainty in these two values. We also included in a black horizontal line, the value of [Fe/H] for the UMA cluster (A. M. Boesgaard et al. 1988).

0.04 dex, GALAH DR3: 0.06, and RAVE DR6: 0.2 dex. When using only stars from the APOGEE DR17 catalog, the scatter in [Fe/H] is reduced to 0.17 dex, although there are only 18 stars. Figure 5 shows in dark purple the distribution of the metallicity for only APOGEE DR17 stars, which clearly shows a smaller scatter for stars with high probability of belonging to the group. This figure also shows that most of the metallicity measurements are within 2σ from the value for UMA, and the stars with small uncertainty that differ from this value have a lower probability of belonging to the CUMA moving group. Last, we calculated the reduced χ-squared for the metallicity values of all the stars and only the stars with a probability higher than 95%, and found 6.32 ($\nu = 61$) and 3.26 ($\nu = 38$), respectively. This shows that high-likelihood members agree better with a single-metallicity population. In conclusion, the distribution of metallicities is consistent with a coeval population.

3.4. C/O Ratio

As a final test of the membership of COCONUTS-2 to CUMA, we used the C/O ratio. This type of comparison has been applied to T dwarfs in wide binaries with main-sequence stars (M. R. Line et al. 2015; M. W. Phillips et al. 2024), and planetary-mass objects (K. K. W. Hoch et al. 2023). There is currently no measurement of the C/O ratio of COCONUTS-2 A, therefore we leveraged the additional members of CUMA. Taking advantage of the abundances compiled for the members of CUMA described above, we used [C/Fe] and [O/Fe] to estimate C/O. Using that the standard definition of abundances is

$$[X_1/X_2] = \log_{10}\left(\frac{N_{X_1}}{N_{X_2}}\right)_{star} - \log_{10}\left(\frac{N_{X_1}}{N_{X_2}}\right)_{\odot},$$
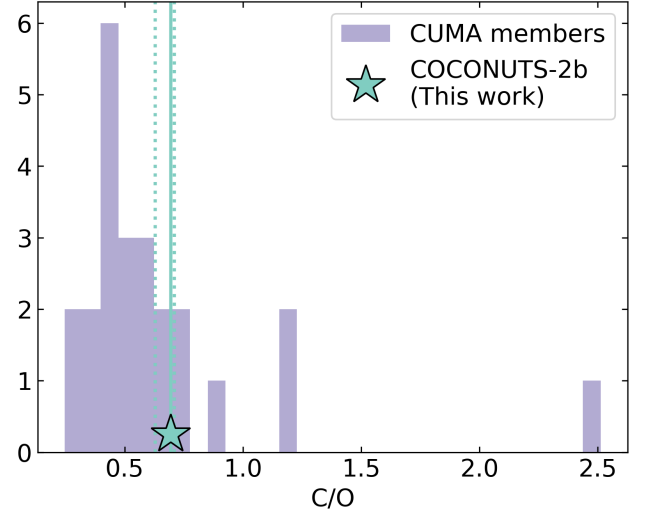

Figure 6. C/O ratio measurements for the members of CUMA. These measurements were estimated from the [C/Fe] and [O/Fe] abundances from the APOGEE DR17 and GALAH DR3 catalogs. We included in a vertical line the C/O ratio result for COCONUTS-2 b from the forward-modeling analysis in this paper (see Section 5.2), which agrees with the values from the group. This suggests that COCONUTS-2 b is a member of CUMA, and also it is likely to have formed in the same mechanism as a star.

we derived that

$$C/O = \frac{N_C}{N_O} = \frac{10^{[C/Fe]+[Fe/H]+\log_{10}\left(\frac{N_C}{N_H}\right)_{\odot}}}{10^{[O/Fe]+[Fe/H]+\log_{10}\left(\frac{N_O}{N_H}\right)_{\odot}}},$$

where $\log_{10}(N_C/N_H)_{\odot} = 8.43 - 12$, and $\log_{10}(N_O/N_H)_{\odot} = 8.69 - 12$ (M. Asplund et al. 2009). Using this method we obtained 24 measurements of C/O ratio for the sample. We show the results from the estimation of C/O for the members of CUMA in Figure 6, and compiled in Table 2. Similar to the metallicity analysis in Section 3.3, we found that most of the values of C/O group around the solar value of 0.55 ± 0.10 (M. Asplund et al. 2009), with some outliers which have large uncertainties (SNR < 2).

COCONUTS-2 b has a measured C/O ratio from Z. Zhang et al. (2025), who performed a forward-modeling analysis of the Gemini/FLAMINGOS-2 spectrum, and found a result close to the solar value ($0.505^{+0.007}_{-0.004}$). In our work, we combined the Gemini/FLAMINGOS-2 spectrum with our JWST spectrum to compare to models. With the unconstrained fit, we found C/O = $0.69^{+0.02}_{-0.07}$, which is consistent within 2σ with the solar value, and with the distribution of values in CUMA. We found that given the uncertainties in the JWST spectrum, our result is compatible with the solar value. We discuss this analysis further in Section 5.2. We show our result for the C/O ratio together with the distribution of values for CUMA in Figure 6. In addition, B. Lacy et al. (2025, in preparation) performed a similar analysis for COCONUTS-2 b using both the Gemini/FLAMINGOS-2 and JWST spectra, but using a different forward-modeling code, and found a solar C/O ratio (private communication). Furthermore, there is an upcoming paper by J. Copeland et al. (2025, in preparation) that will present the results from the retrieval analysis for this object.
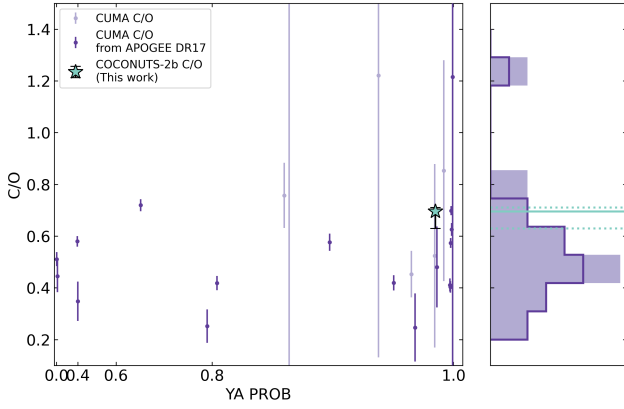
Figure 7. We show in the left panel C/O ratio measurements for the members of CUMA as a function of the probability of each candidate to belong to the CUMA group, and in the right panel a histogram of the values. We also show as a five-point star in the left panel, and as a horizontal line in the right panel, our result for the C/O ratio for COCONUTS-2 b from the forward-modeling analysis.

In order to study the intrinsic scatter of the C/O measurements, we made Figure 7. We show in the left panel of the figure the values of the C/O ratio as a function of the probability of belonging to the CUMA group, and in the right panel the distribution of values. We included the value for COCONUTS-2 b as a five-point star in the left panel and as a horizontal line in the right panel. This figure shows that the values that deviate from the solar C/O ratio have the largest uncertainty. We also estimated the reduced χ-squared value for the C/O values of all the stars and only the stars with a probability higher than 95%, and found 1.34 ($\nu = 23$) and 1.05 ($\nu = 12$), respectively. This shows that the population is consistent with a constant C/O ratio value.

The agreement of the C/O ratio of COCONUTS-2 b with the members of CUMA supports its membership to the group. The C/O ratio also works as an indicator of the formation of the system. Planets that formed beyond the water snowline can have high values of C/O, even if the star has a solar C/O ratio (N. Madhusudhan et al. 2011; K. I. Öberg et al. 2011). Therefore, our results also suggest that COCONUTS-2 b formed in the same mechanism as a star, supporting previous results (Z. Zhang et al. 2021a, 2025).

4. Luminosity, Effective Temperature, Mass, Radius, and Surface Gravity Estimation

Combining the spectra described in Section 2.1 and the photometry described in Section 2.2, we used SEDkit[26] (J. C. Filippazzo et al. 2015; J. Filippazzo et al. 2025) to estimate bolometric luminosity (L_{bol}), mass, radius, surface gravity ($\log g$), and effective temperature (T_{eff}) for both components of COCONUTS-2. Below, we provide a brief description of how the code estimates each parameter, followed by detailed explanations for COCONUTS-2 A and COCONUTS-2 b, as well as the results.

SEDkit combines the input data and extrapolates the missing flux at short and long wavelengths using Wien's approximation and the Rayleigh–Jeans (RJ) law, respectively, using an initial guess for T_{eff}, to compile a complete SED. SEDkit then integrates this full SED to calculate the

---

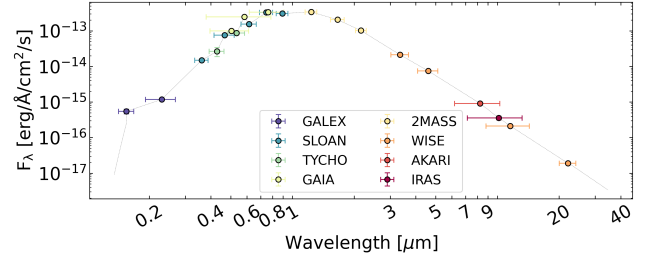[26] https://github.com/BDNYC/sedkit/tree/main

Figure 8. SED for COCONUTS-2 A. We obtained the photometry from the literature (see Section 2.2). The gray line represents the connecting lines, as well as the Wien and RJ approximations, extending beyond the existing data.

bolometric flux and the bolometric luminosity using the parallax measurement. Combining L_{bol} with the age estimated from CUMA (see Section 3) and a choice of evolutionary models, the code estimates mass, radius, and $\log g$, and it estimates T_{eff} from the radius and luminosity using the Stefan–Boltzmann Law. We also estimated $\log L_{bol}/L_\odot$ assuming a solar luminosity of 3.828×10^{33} erg s^{-1}. The uncertainty of the bolometric flux (F_{bol}) is determined using Monte Carlo propagation, accounting for the flux and photometry uncertainties, assuming Gaussian distributions. Then the uncertainty of L_{bol} is propagated from errors in F_{bol} and distance. Finally, the value and uncertainties for the rest of the parameters are estimated using a modification we added to SEDkit: the new code does a Monte Carlo propagation of uncertainties from normal distributions for the age and L_{bol}. Using the interpolation of the evolutionary models done with LinearNDInterpolator from scipy, it obtains a distribution for each of the other parameters.

4.1. COCONUTS-2 A

We assumed a $T_{eff} = 3406$ K for the M3 component of the system for the Wien and RJ approximations, based on the value calculated by E. Gaidos et al. (2014). To take into account model uncertainty in our parameter estimation, we used two different sets of evolutionary models: the MESA Isochrones and Stellar Tracks (B. Paxton et al. 2011, 2013, 2015, 2018; J. Choi et al. 2016; A. Dotter 2016) and the I. Baraffe et al. (2015) models. The final value for each parameter is calculated as the average of the results from each model, with the uncertainty determined through error propagation. In both cases we used nonrotating, solar-metallicity models. We show our results in Table 1, and in Figure 8 with a gray line showing the connecting lines used to interpolate the photometry points and calculate the bolometric luminosity. In addition, the gray line indicates the RJ and Wien approximations to extrapolate our data to low and high frequencies, respectively, where no data are available, as explained above in the short description of SEDkit. Our results are consistent within 1σ with previous studies (E. Gaidos et al. 2014; Z. Zhang et al. 2021a) with an improvement of around 50% in the uncertainties in most of the parameters due to our more complete SED, except for radius where they stay equal.

4.2. COCONUTS-2 b

We used an initial guess for T_{eff} of the T9 component of COCONUTS-2 of 483 K for the Wien and RJ approximations, based on the calculations from Z. Zhang et al. (2025). We also used the Sonora–Bobcat evolutionary models for solar
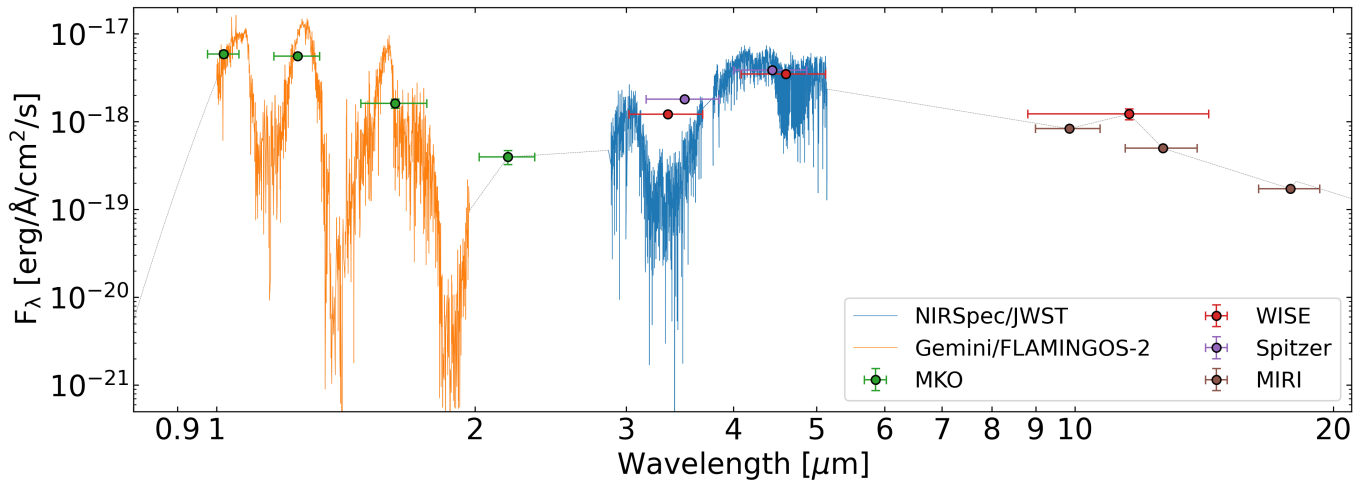
Figure 9. SED for COCONUTS-2 b. We show in orange the Gemini/FLAMINGOS-2 spectrum (Z. Zhang et al. 2025), in blue the G395H NIRSpec JWST spectrum, and in brown points the MIRI photometry. We also included photometry from the literature. MKO label (green, in increasing wavelength): Gemini/FLAMINGOS-2 Y, J_{MKO} (NSFCam J), H_{MKO} (NSFCam H), and K_{MKO} (NSFCam K); WISE label (red): W1 (WISE W1), W2 (WISE W2), and W3 (WISE W3); Spitzer label (purple): [3.6] (IRAC I1) and [4.5] (IRAC I2); and MIRI label (brown): MIRI F1000W, MIRI F1280W, and MIRI F1800W. See Table 1 for the magnitude of each photometry point. The gray line represents the connecting lines, as well as the Wien and RJ approximations, extending beyond the existing data.

metallicity (M. S. Marley et al. 2021) to estimate the parameters of COCONUTS-2 b using SEDkit. We show our results in Table 1, and the compilation of data together with the approximations in Figure 9. The Gemini and JWST data account for 48% of the bolometric flux, which increases to 68% when including the three MIRI photometry points. The parameters we estimated are within $1\sigma-2\sigma$ from previous studies (Z. Zhang et al. 2021a, 2025), but we found an L_{bol} almost 4% larger, which affected the rest of the parameters resulting in a higher mass and higher temperature.

In Section 2.2 we discussed a systematic offset between the literature values of W1 and [3.6], and the synthetic photometry. We found that the synthetic photometry is 0.5 mag fainter than the literature value. Given that Z. Zhang et al. (2021a, 2025) used literature photometry to estimate L_{bol} in this wavelength range, this would cause our luminosity to be fainter in comparison with their results. However, as we found the opposite effect, we conclude that the systematic difference is not strong enough to make a difference in the resulting values.

5. Atmospheric Composition

The strategically selected band of JWST high-resolution spectra allows us to study COCONUTS-2 b's atmospheric composition in detail, given that several dominant gaseous molecules absorb at these wavelengths, such as CH_4, CO, and CO_2. In this section we present the JWST spectrum of COCONUTS-2 b, compare it to different molecular opacities to identify the molecules present in the atmosphere, and perform a forward-modeling analysis. Finally we compared our results to WISE J082507.35+280548.5, another object from the JWST GO 2124 program, which we find is a candidate member of CUMA.

5.1. Molecules in the Atmosphere of COCONUTS-2 b

We performed a detailed inspection of the JWST spectrum as shown in the top panel of Figure 1, where the resolution and precision of the JWST spectrum allowed us to interpret each of the features. In order to identify each molecule, we

used opacities from The Data and Analysis Center for Exoplanets (DACE),[27] which we retrieved using the package dace-query.[28] The DACE database contains opacities for different molecules, which were calculated using the open-source code HELIOS-K (S. L. Grimm et al. 2021). HELIOS-K estimates the opacities using molecular lines from different databases. For our work we used opacities for CO, CO_2, and CH_4, which were calculated with the molecular lines from HITEMP (L. S. Rothman et al. 2010; R. J. Hargreaves et al. 2020). In addition we included opacities for H_2O and NH_3, which were calculated from the molecular lines included in the ExoMol database (R. J. Barber et al. 2006; S. N. Yurchenko et al. 2011; A. A. A. Azzam et al. 2016; J. Tennyson et al. 2024). We show the opacities for these molecules in the bottom panel in Figure 1, assuming a temperature of 450 K and a pressure of 0.1 bar. By comparing the opacities to the JWST spectrum, we see clear features of NH_3, CH_4, CO_2, CO, and H_2O, which we marked approximately in the top panel of Figure 1. We found clear narrow absorption features of NH_3 in the range [3.0, 3.1] μm, and a broad absorption feature is generated by CH_4 in the range [3.1, 4.15] μm, which is the dominant feature in the spectral range we observed. In addition, there are clear wide absorption features from CO_2 and CO in the ranges [4.17, 4.44] μm and [4.44, 4.9] μm, respectively. There is clear overlap of the CO feature with the H_2O narrow absorption features in the range [4.8, 5.13] μm, and we further identify similar water signals in the range [2.87, 3.0] μm.

5.2. Forward Modeling

We conducted a forward-modeling analysis of the data available for COCONUTS-2 b, to study the atmospheric properties of this object. In this work, we fit the Gemini/FLAMINGOS-2 spectrum, analyzed by Z. Zhang et al. (2025), together with our JWST spectrum. For our analysis we used four atmospheric model grids: ATMO2020++ (S. K. Leggett et al. 2021; A. M. Meisner et al. 2023), PH_3-free ATMO2020++

---

[27] https://dace.unige.ch/opacity/
[28] https://dace-query.readthedocs.io/en/latest/index.html

Table 3
Models Included in the Forward-modeling Analysis of COCONUTS-2 b

Atmospheric Model	$T_{\rm eff}$ (K)	$\log g$ (dex)	[M/H] (dex)	C/O	$\log(K_{\rm zz})$ (cm^2 s^{-1})
ATMO2020++	250:1200	2.5:5.5	−1:0.3	0.55	6.0
no PH$_3$	250:1200	2.5:5.5	−1:0.3	0.55	6.0
Sonora Elf Owl	275:2400	3:5.5	−1:1	0.5:2.5	2:9
LB23	250:800	3.5:5	−0.5:0.5	0.537	6.0

(S. K. Leggett & P. Tremblin 2024), Sonora Elf Owl version 2 (S. Mukherjee et al. 2024, 2025), and the B. Lacy & A. Burrows (2023, hereafter LB23) models. We performed the forward modeling in a Bayesian framework using SEDA (G. Suárez et al. 2021),[29] an open-source Python package for the forward modeling, and analysis of SEDs of ultracool objects and directly imaged exoplanets. In this package, the sampling of the posterior is done using dynamic nested sampling (J. Skilling 2004, 2006), which was implemented in the package dynesty (J. S. Speagle 2020; S. Koposov et al. 2024).[30] SEDA estimates the best fit from an interpolated grid of models without any prior information from evolutionary models. We refer to the results in B. Lacy et al. (2025, in preparation), who performed a fit of COCONUTS-2 b also combining the Gemini/FLAMINGOS-2 spectrum with the JWST spectrum, but assuming the Sonora–Bobcat evolutionary models (M. S. Marley et al. 2021) to constrain the parameters.

5.2.1. Models Included

Here we briefly discuss the models selected for our analysis, and we refer to their individual publications for a more detailed description. We show a summary of all the models included in our analysis in Table 3. ATMO2020++ is based on the ATMO2020 framework (M. W. Phillips et al. 2020), which assumes radiative–convective equilibrium, solar metallicity, and cloud-free atmospheres. ATMO2020++ adds nonadiabatic thermal structure in the model grid, and includes metallicity as a grid parameter. Therefore it contains a grid of effective temperature, surface gravity, and metallicity in the following ranges: $T_{\rm eff} = [250, 1200]$ K, $\log g = [2.5, 5.5]$ dex, and [M/H] = [−1, 0.3] dex. The PH$_3$-free grid shares these assumptions, but excludes phosphine. Both ATMO2020++ and the PH$_3$-free grid assume a solar C/O ratio, and a diffusion coefficient of $K_{\rm zz} = 10^6$ cm^2 s^{-1}. The assumed model parameters are indicated in Table 3 and in Table 4 in parenthesis.

The Sonora Elf Owl model grid builds on the Sonora–Bobcat model grid (M. S. Marley et al. 2021), which assumes radiative–convective equilibrium, rainout equilibrium chemistry, and cloud-free atmospheres, by incorporating disequilibrium chemistry, and an expanded range of [M/H] and C/O. The grid of the Sonora Elf Owl models covers the ranges of $T_{\rm eff} = [275, 2400]$ K, $\log g = [3, 5.5]$ dex, $\log(K_{\rm zz}) = [2, 9]$ dex, [M/H] = [−1, 1] dex, and C/O = [0.5, 2.5].

Last, the LB23 models assume radiative–convective equilibrium, and span cloud-free, cloudy, equilibrium, and disequilibrium conditions. The grid of the LB23 models covers the ranges $T_{\rm eff} = [250, 800]$ K, $\log g = [3.5, 5]$, and [M/H] = [−0.5, 0.5],

and varying mixing lengths $H_{\rm mix} = [0.01, 1]$, assuming a solar C/O ratio and $K_{\rm zz} = 10^6$ cm^2 s^{-1}.

For each of the models described above, SEDA adds the radius of the object as a free parameter, which is estimated from the scaling factor required to match the model with the observed data, and the distance to the object.

5.2.2. Constrained versus Unconstrained Fits

We performed the forward-modeling analysis with two different sets of priors: (1) unconstrained with loose priors on the ranges for the parameters: $T_{\rm eff} = [400, 700]$ K, $\log g = [3.0, 5.0]$ dex, and [M/H] = [−0.5, 0.5] dex; and (2) constrained with fixed values for $T_{\rm eff}$ and $\log g$, where we selected the value from the grid of each model closest to the results from the SED fitting (see Section 4). For both cases, we assumed a wide range of possible radii between [0.7, 1.2] $R_{\rm Jup}$. The fix values are indicated in Table 4 in parenthesis. As SEDA does not assume evolutionary models to perform the fit, the constrained parameters allow us to identify the best fit assuming the age of the system (414 ± 23 Myr, see Section 3). The results of the fit for both case scenarios are shown in Table 4, where we indicate the resulting reduced χ-squared (χ_ν^2) and the degrees of freedom (ν) for each model. In both cases we found that the best-fit model is the Sonora Elf Owl. This result differs from the results of Z. Zhang et al. (2025), who performed a forward-modeling analysis of the Gemini/FLAMINGOS-2 spectrum, where the PH$_3$-free ATMO2020++ models were preferred.

For the unconstrained fit we found that the effective temperature is consistent within 2σ for most of the fits with the SED fit result ($T_{\rm eff} = 493 \pm 9$ K), while the surface gravity is much lower (SED result: $\log g = 4.17 \pm 0.02$ dex). This differs from the results from Z. Zhang et al. (2025), who found surface gravities compatible with the SED results, but agrees with the results from B. Lacy et al. (2025, in preparation). Given that the uncertainty of the JWST spectrum is significantly lower than the Gemini/FLAMINGOS-2 spectrum (see Section 2.1), our fit is dominated by the JWST spectrum, indicating that the later is driving the difference in the results. In addition, we found that for both the constrained and unconstrained fits we obtained radii close the the 1 $R_{\rm Jup}$ expected for brown dwarfs (A. Burrows & J. Liebert 1993; A. Burrows et al. 1997), although our results are slightly smaller. This difference is probably due to the fact that in our fits the radius is a free parameter, instead of being constrained by evolutionary models.

For the metallicity measurement, we found that both in the constrained as in the unconstrained cases the value of [M/H] is subsolar, with the unconstrained case resulting in a slightly more metal-poor result. These results are consistent with the results in Z. Zhang et al. (2025).

Lastly, we obtained a C/O ratio slightly higher than solar for the unconstrained case ($0.69^{+0.02}_{-0.07}$), and even higher for the constrained case ($0.87^{+0.08}_{-0.01}$). Both Z. Zhang et al. (2025) and B. Lacy et al. (2025, in preparation) found a solar C/O ratio for COCONUTS-2 b. To study this difference in detail, we compared the JWST spectrum flux and uncertainty to different Sonora Elf Owl models, fixing all the parameters to the best fit indicated in Table 4, and varying only the C/O ratio. We found that given the uncertainty of the JWST spectrum, we cannot distinguish between the solar C/O ratio and the case of C/O = 0.7, but we can distinguish the case of C/O = 0.8.

[29] https://seda.readthedocs.io/en/latest/
[30] https://dynesty.readthedocs.io/en/v2.1.5/

Table 4
Forward-modeling Results for COCONUTS-2 b

Atmospheric Model	χ^2_ν	ν	$T_{\rm eff}$[a] (K)	$\log g$ (dex)	[M/H] (dex)	C/O	$\log(K_{zz})$ (cm² s⁻¹)	R ($R_{\rm Jup}$)
				Unconstrained				
Sonora Elf Owl	4.24	4105	$516.61^{+5.83}_{-1.90}$	$3.251^{+0.001}_{-0.087}$	$-0.337^{+0.016}_{-0.046}$	$0.69^{+0.02}_{-0.07}$	$4.43^{+0.13}_{-0.13}$	$0.846^{+0.011}_{-0.019}$
LB23	8.47	4105	$500.00^{+0.34}_{-0.36}$	$3.549^{+0.006}_{-0.031}$	$-0.480^{+0.005}_{-0.056}$	(0.537)	(6.0)	$0.818^{+0.002}_{-0.015}$
ATMO2020++ no PH$_3$	10.11	4107	$528.67^{+1.12}_{-4.91}$	$4.010^{+0.006}_{-0.107}$	$-0.332^{+0.008}_{-0.056}$	(0.55)	(6.0)	$0.779^{+0.017}_{-0.005}$
ATMO2020++	11.1	4107	$512.03^{+1.77}_{-1.17}$	$3.736^{+0.009}_{-0.054}$	$-0.492^{+0.006}_{-0.123}$	(0.55)	(6.0)	$0.883^{+0.007}_{-0.009}$
				Constrained				
Sonora Elf Owl	7.53	4105	(500.0)	(4.25)	$-0.179^{+0.004}_{-0.046}$	$0.87^{+0.08}_{-0.01}$	$4.03^{+0.42}_{-0.03}$	$0.825^{+0.002}_{-0.003}$
LB23	9.43	4105	(500.0)	(4.25)	$-0.239^{+0.008}_{-0.005}$	(0.537)	(6.0)	$0.833^{+0.002}_{-0.002}$
ATMO2020++ no PH$_3$	11.14	4107	(500.0)	(4.0)	$-0.177^{+0.004}_{-0.004}$	(0.55)	(6.0)	$0.931^{+0.002}_{-0.002}$
ATMO2020++	11.58	4107	(500.0)	(4.0)	$-0.170^{+0.004}_{-0.004}$	(0.55)	(6.0)	$0.972^{+0.002}_{-0.002}$

Note.
[a] Numbers in parenthesis indicate that the parameter is fixed in the model or the fit.

Therefore we concluded that for the unconstrained case, our results are compatible with a solar C/O ratio, while for the constrained one they are not. This result is due to features such as CH$_4$, CO, and CO$_2$, which are sensitive to the C/O ratio, $T_{\rm eff}$, and $\log g$. Therefore, fixing the two latter parameters affects the result of the C/O ratio.

5.3. Comparison to a Candidate Member of CUMA: WISE J082507.35+280548.5

In this section, we compare COCONUTS-2 b to another object from the JWST GO 2124 program: WISE J082507.35+280548.5 (hereafter 0825+2805), a Y0.5 dwarf discovered by A. C. Schneider et al. (2015). By using BANYAN Σ with the radial velocity measurement for 0825+2805 (-18.7 ± 3.4 km s⁻¹; J. K. Faherty et al. 2025, in preparation; see Section 3 for a description of the calculation) together with the PM and parallax (PM R. A. = -66.7 ± 0.9 mas yr⁻¹, PM decl. = -235.8 ± 0.9 mas yr⁻¹, and Parallax: 155.8 ± 2.4 mas; J. D. Kirkpatrick et al. 2021), we calculated a probability of 93% of belonging to CUMA. This percentage, although high, indicates a lower probability of belonging to CUMA than found for COCONUTS-2. 0825+2805 has a radial velocity measurement with a 20% uncertainty, which given our calculations in Section 3.1, indicates that the probability of chance alignment is 1 in 89. Therefore 0825+2805 is good candidate member of CUMA.

M. J. Rowland et al. (2025, in preparation) performed a retrieval analysis on the JWST spectrum of 0825+2805, and found that it has solar metallicity and a solar C/O ratio (private communication). These measurements agree with the rest of the members of CUMA (see Section 3), which support the membership we calculated using kinematics. Although more information is needed to confirm the membership of 0825+2805 to CUMA, the analysis done in this paper is enough to assume the membership for the rest of this section. Therefore, 0825+2805 is a free-floating object that, as a candidate member of CUMA, is likely to have the same age as COCONUTS-2 b. In addition, both objects have similar metallicities (with COCONUTS-2 b being slightly subsolar) and C/O ratios, making the comparison of the JWST spectra of the two objects interesting.

We combined the JWST/NIRSpec spectrum and the three MIRI photometry points obtained as part of the JWST GO 2124 program with the data available in the literature, which includes a spectrum from the Hubble Space Telescope WFC3 (A. C. Schneider et al. 2015), and photometry (J. D. Kirkpatrick et al. 2021), to measure the bolometric luminosity of 0825+2805 using SEDkit. Following the same method as described in Section 4, we used an initial guess temperature of 350 K (S. K. Leggett & P. Tremblin 2024) to add the long- and short-wavelength approximations where data were not available. Assuming the age of CUMA, we estimated an effective temperature of $T_{\rm eff} = 359 \pm 3$ K, a surface gravity of $\log g = 3.85 \pm 0.02$ dex, a mass of $M = 3.7 \pm 0.2\,M_{\rm Jup}$, and a radius of $R = 1.144 \pm 0.002\,R_{\rm Jup}$. Therefore, assuming the membership of 0825+2805 to CUMA, we found that it is a free-floating planetary-mass object. This shows that CUMA is a good target for follow-up using the Nancy Grace Roman Space Telescope to study the population of free-floating planetary-mass objects.

As mentioned above, comparing 0825+2805 and COCONUTS-2 b presents a unique opportunity to isolate the effect of mass on brown dwarf evolution, since the two objects have similar ages and metallicities. We show the JWST spectra of COCONUTS-2 b and 0825+2805 in Figure 10. We divided the spectra in three panels, and normalized each panel separately to facilitate the comparison of the different molecular features. In addition, we included the opacities for the relevant molecules in the atmospheres of these two objects (H$_2$O, CO, CO$_2$, CH$_4$, and NH$_3$). We found that the feature of H$_2$O in the range [4.8, 5.13] μm and CH$_4$ in the range [3.1, 4.15] μm are deeper for 0825+2805 than for COCONUTS-2 b, which indicates that the atmosphere of 0825+2805 has higher abundances of H$_2$O and CH$_4$ than COCONUTS-2 b. In addition, we found that the features of CO$_2$ in the range [4.17, 4.44] μm and CO in the range [4.44, 4.9] μm have similar depths, which indicates that the abundances are similar in both objects. For this analysis we are assuming that the temperature–pressure profiles of both objects are similar. A retrieval analysis of both objects is required to confirm that the depths of the feature can be directly related with the abundances.

We used the Sonora Elf Owl models to study the evolution of the molecular features discussed above with mass at a fixed age. We fixed the age to the age of CUMA, the metallicity and C/O ratio to the solar values, the $\log(K_{zz})$ to 4.0 dex, and
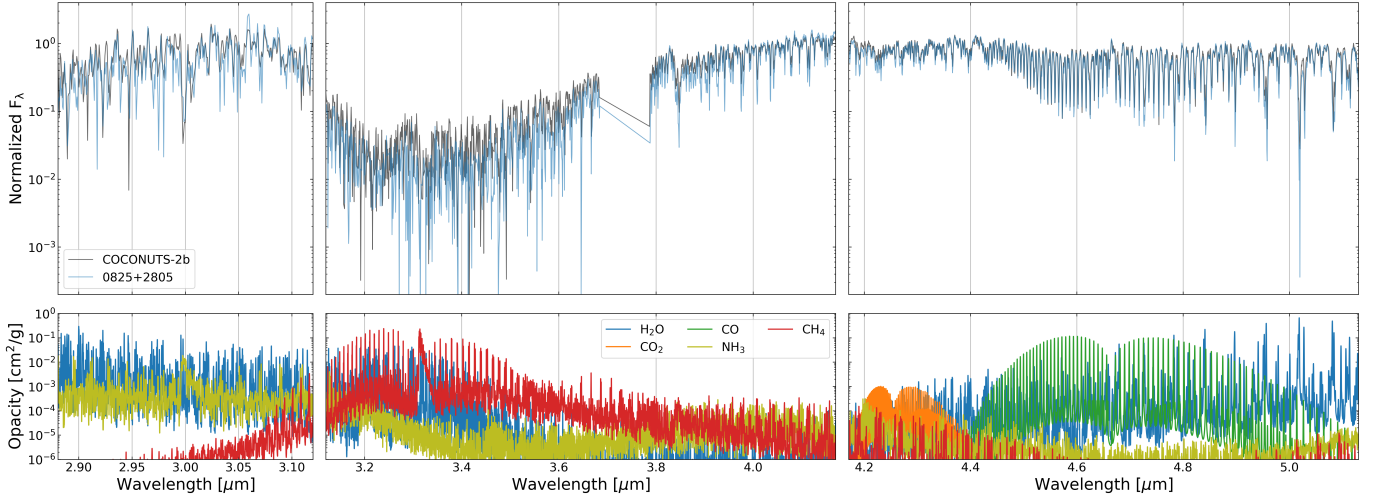
Figure 10. Comparison of the G395H NIRSpec JWST spectra of COCONUTS-2 b and 0825+2805 from the JWST GO 2124 program. In this figure, each of the three panels is normalized separately to facilitate the comparison to molecule abundances. Assuming that both objects have similar temperature–pressure profiles, we found that the abundances of H_2O and CH_4 in the atmosphere of COCONUTS-2 b are lower than for 0825+2805, which agrees with 0825+2805 being less massive and colder. We also found that the abundances of CO and CO_2 are consistent, which is consistent with COCONUTS-2 b have lower metallicity and it might indicate that the vertical mixing of 0825+2805 is stronger to compensate the effects of mass and temperature.

changed the effective temperature and surface gravity with mass assuming the Sonora–Bobcat evolutionary models. We found that for more massive brown dwarfs (comparing from 4 $M_{\rm Jup}$ to 10 $M_{\rm Jup}$), the effective temperature increases (from approximately 371 to 591 K) and the surface gravity increases (from approximately 4.06 to 4.3 dex), the CH_4 and H_2O features shallow, while those of CO and CO_2 are deep. Given that 0825+2805 is less massive and colder than COCONUTS-2 b, this could explain that the abundances of CH_4 and H_2O are higher for the former.

We also left all the parameters fixed to the values of COCONUTS-2 b and changed only the metallicity from −0.4 dex to solar metallicity, and found that while CH_4 and H_2O do not change significantly, metal-poor objects have lower CO and CO_2 abundances than the solar-metallicity objects. Therefore the difference in metallicity between COCONUTS-2 b and 0825+2805 might explain why the abundances of CO and CO_2 are similar for both objects, given that it compensates for the effects of mass and temperature.

Finally, we explored fixing all the parameters to the values of COCONUTS-2 b, and changing only $\log(K_{\rm zz})$ from 4 to 8 dex. We found that CO and CO_2 deepen with stronger mixing, while CH_4 gets shallower, as it was pointed out by S. Mukherjee et al. (2024). Therefore, this would indicate that the vertical mixing of 0825+2805 is stronger than that of COCONUTS-2 b, given that it compensates for the effects of mass and temperature in the abundances. This analysis shows the importance of benchmark brown dwarfs that belong to moving groups, which can be used to study atmospheric properties such as vertical mixing and metallicity.

6. Conclusions

In this work we study the COCONUTS-2 system, which is a wide binary, composed of an M3 star and a T9 brown dwarf. COCONUTS-2 b is part of the JWST GO 2124 program, which obtained a NIRSpec spectrum with the G395H disperser, in the range [2.87, 5.13] μm, and three bands of MIRI photometry: F1000W (8.8−11.1 μm), F1280W (11.3−14.3 μm), and F1800W (16.0−20.3 μm). We used the new MIRI images to update the position, proper motions, and parallax of COCO-NUTS-2 b. Taking advantage of the full kinematics of COCO-NUTS-2 A from Gaia, and our new astrometry together with the radial velocity obtained from the JWST spectrum for COCO-NUTS-2 b (J. K. Faherty et al. 2025, in preparation), we found that the COCONUTS-2 system is likely a member of the CUMA moving group, supporting previous results (F. Marocco et al. 2024). We further supported this membership by calculating the probability of chance alignment, measuring rotation periods for the group, and compiling metallicity and C/O ratio measurements for the members of CUMA. We found that the distributions are centered at solar values for both the metallicity and C/O ratio. By performing a forward-modeling analysis of COCONUTS-2 b, we found that is has a C/O ratio compatible with solar, and a slightly subsolar metallicity. By comparing the literature measurement of metallicity for COCONUTS-2 A, and the results from the forward modeling for COCONTS-2 b, we found good agreement between the system and the members of CUMA, supporting their membership. In addition, given that COCONUTS-2 b has a C/O ratio consistent with the rest of the members of CUMA, it likely formed with the same mechanism as a star, supporting previous results (Z. Zhang et al. 2021a, 2025).

Using the new JWST/NIRSpec spectrum and MIRI photometry combined with a Gemini/FLAMINGOS-2 spectrum (Z. Zhang et al. 2025) and photometry from the literature (J. D. Kirkpatrick et al. 2021), we used SEDkit to estimate the bolometric luminosity, mass, effective temperature, surface gravity, and radius of COCONUTS-2 b, assuming its age is that of the moving group. We found that COCONUTS-2 b is a planetary-mass object of 7.5 ± 0.4 $M_{\rm Jup}$. In addition, by comparing the JWST spectrum with molecular opacities, we find clear evidence for the presence of NH_3, CH_4, CO_2, CO, and H_2O in the atmosphere of COCONUTS-2 b.

Finally we compared COCONUTS-2 b to 0825+2805, a Y0.5 dwarf discovered by A. C. Schneider et al. (2015), which we found is a potential member of CUMA (93% probability), and is also part of the JWST GO 2124 program. Furthermore, by doing a retrieval analysis of 0825+2805, M. J. Rowland et al. (2025, in preparation) found solar values for its

metallicity and C/O ratio (private communication), which are similar to our forward-modeling results for COCONUTS-2 b, making these two objects interesting for comparison of their spectra. Assuming that the age of 0825+2805 is that of CUMA, we found that it is a cold (359 ± 3 K) planetary-mass object ($3.7 \pm 0.2 M_{\rm Jup}$). By comparing the G395H NIRSpec JWST spectra for 0825+2805 with COCONUTS-2 b, and assuming both objects have similar temperature–pressure profiles, we found that the former has higher abundances for H_2O and CH_4, which agrees with the fact that it is a colder and less massive object. In addition we found that both objects have CO and CO_2 features with similar depths, which could be a result of COCONUTS-2 b being slightly more metal poor, and/or could indicate that the vertical mixing is stronger for 0825+2805, to compensate for the effects of temperature and mass.

Author Contributions

R.K. performed most of the analysis for this work, coordinated the collaboration with coauthors, and was responsible for writing and submitting the manuscript.

C.A.B. provided guidance and regular feedback during the development of the project, as well as funding for this project.

A.R.D. together with R.K. were responsible for the forward-modeling analysis and writing that section in the manuscript.

J.K.F. provided regular feedback during the development of the project, and helped to coordinate the collaboration between coauthors. J.K.F. is also the PI of the JWST GO program that obtained the spectrum and photometry for the objects studied in this work.

B.L. and G.S. provided valuable guidance with the forward-modeling analysis, model comparison, and analysis of molecule abundances. Both coauthors contributed to refining the manuscript through detailed reviews.

J.D.K. and F.M. estimated the new astrometry for COCONUTS-2 b, and F.M. was responsible for writing Section 2.3, describing this analysis.

J.G. provided valuable feedback on the membership analysis using Banyan Σ, and the tests done to estimate the chance alignment.

J.C. and B.B. added significant discussion on the composition of the atmosphere of COCONUTS-2 b, by comparing the results from this work with the retrieval analysis they are doing.

N.W. helped with the forward-modeling analysis by mentoring A.R.D. at the beginning of the project.

M.J.R. improved significantly the comparison to the 0825+2805 object by sharing the results from the retrieval analysis, and discussing the results from the forward modeling of COCONUTS-2 b.

D.C.B.G., J.M.V., A.C.S., and E.C.G. improved the manuscript significantly with a thorough review of the text, and provided insightful comments which improved the work.

S.A.M. provided valuable feedback on the estimation of bolometric luminosity of the object and development of SEDkit.

A.R. improved the manuscript significantly with a thorough review of the text.

R.S., E.C., and R.A.M. were responsible for obtaining the data we used in this work to estimate the astrometry of COCONUTS-2 b.

Software: astropy (Astropy Collaboration et al. 2013, 2018, 2022); ChronoFlow (P. R. Van-Lane et al. 2025); dace-query; dynesty (J. S. Speagle 2020; S. Koposov et al. 2024); emcee (D. Foreman-Mackey et al. 2013); imcore; matplotlib (J. D. Hunter 2007); mpfit (C. B. Markwardt 2009); numpy (C. R. Harris et al. 2020); PypeIt (J. X. Prochaska et al. 2020a, c, 2020b); SEDA (G. Suárez et al. 2021); SEDkit (J. C. Filippazzo et al. 2015; J. Filippazzo et al. 2025); scipy (P. Virtanen et al. 2020).

Appendix
Comparison with the Previous Gemini/FLAMINGOS-2 Reduction

We compared the reduction of the Gemini/FLAMINGOS-2 data done by Z. Zhang et al. (2025), available online,[31] with our reduction done with PypeIt, and the results are shown in Figure 11. We found in general good agreement between the two reductions. The areas where the two spectra differ most (around 1, 1.4, and 1.9 μm) correspond to wavelength ranges where the telluric contamination is high, and the uncertainty of the flux is high. The spectra are still consistent within the uncertainties. As the fit to the data was done using the uncertainties in the fluxes as a weight in both studies, these differences should not affect the results.
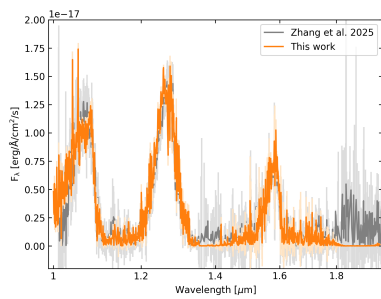
---

[31] https://zenodo.org/records/13975825

Figure 11. Comparison of our reduction of the Gemini/FLAMINGOS-2 data with the original from Z. Zhang et al. (2025).

ORCID iDs

Rocio Kiman ⓘ https://orcid.org/0000-0003-2102-3159
Charles A. Beichman ⓘ https://orcid.org/0000-0002-5627-5471
Azul Ruiz Diaz ⓘ https://orcid.org/0000-0001-6733-4118
Jacqueline K. Faherty ⓘ https://orcid.org/0000-0001-6251-0573
Brianna Lacy ⓘ https://orcid.org/0000-0002-9420-4455
Genaro Suárez ⓘ https://orcid.org/0000-0002-2011-4924
Federico Marocco ⓘ https://orcid.org/0000-0001-7519-1700
J. Davy Kirkpatrick ⓘ https://orcid.org/0000-0003-4269-260X
Jonathan Gagné ⓘ https://orcid.org/0000-0002-2592-9612
Jessica Copeland ⓘ https://orcid.org/0009-0005-7267-7760
Ben Burningham ⓘ https://orcid.org/0000-0003-4600-5627
Niall Whiteford ⓘ https://orcid.org/0000-0001-8818-1544
Melanie J. Rowland ⓘ https://orcid.org/0000-0003-4225-6314
Daniella C. Bardalez Gagliuffi ⓘ https://orcid.org/0000-0001-8170-7072
Johanna M. Vos ⓘ https://orcid.org/0000-0003-0489-1528
Adam C. Schneider ⓘ https://orcid.org/0000-0002-6294-5937
Eileen C. Gonzales ⓘ https://orcid.org/0000-0003-4636-6676
Sherelyn Alejandro Merchan ⓘ https://orcid.org/0000-0003-0548-0093
Austin Rothermich ⓘ https://orcid.org/0000-0003-4083-9962
Richard Smart ⓘ https://orcid.org/0000-0002-4424-4766
Edgardo Costa ⓘ https://orcid.org/0000-0003-4142-1082
Rene A. Mendez ⓘ https://orcid.org/0000-0003-1454-0596

References

Abdurro'uf, Accetta, K., Aerts, C., et al. 2022, ApJS, 259, 35
Abrahamyan, H. V., Mickaelian, A. M., & Knyazyan, A. V. 2015, A&C, 10, 99
Agüeros, M. A., Bowsher, E. C., Bochanski, J. J., et al. 2018, ApJ, 862, 33
Ahumada, R., Allende Prieto, C., Almeida, A., et al. 2022, yCat, 5154, 0
Alejandro Merchan, S., Faherty, J. K., Suárez, G., et al. 2025, ApJ, 989, 80
Aller, K. M., Liu, M. C., Magnier, E. A., et al. 2016, ApJ, 821, 120
Asplund, M., Grevesse, N., Sauval, A. J., & Scott, P. 2009, ARA&A, 47, 481
Astropy Collaboration, Robitaille, T. P., Tollerud, E. J., et al. 2013, A&A, 558, A33
Astropy Collaboration, Price-Whelan, A. M., Sipőcz, B. M., et al. 2018, AJ, 156, 123
Astropy Collaboration, Price-Whelan, A. M., Lim, P. L., et al. 2022, ApJ, 935, 167
Azzam, A. A. A., Tennyson, J., Yurchenko, S. N., & Naumenko, O. V. 2016, MNRAS, 460, 4063
Baraffe, I., Homeier, D., Allard, F., & Chabrier, G. 2015, A&A, 577, A42
Barber, R. J., Tennyson, J., Harris, G. J., & Tolchenov, R. N. 2006, MNRAS, 368, 1087
Bardalez Gagliuffi, D. C., Faherty, J. K., Suárez, G., et al. 2025, ApJ, 984, 74

Beiler, S. A., Cushing, M. C., Kirkpatrick, J. D., et al. 2024, ApJ, 973, 107
Bianchi, L., Herald, J., Efremova, B., et al. 2011, Ap&SS, 335, 161
Boesgaard, A. M., Budge, K. G., & Burck, E. E. 1988, ApJ, 325, 749
Brasseur, C. E., Phillip, C., Fleming, S. W., Mullally, S. E., & White, R. L., 2019 Astrocut: Tools for Creating Cutouts of TESS Images, Astrophysics Source Code Library, ascl:1905.007
Buder, S., Sharma, S., Kos, J., et al. 2021, MNRAS, 506, 150
Burgasser, A. J., Simcoe, R. A., Bochanski, J. J., et al. 2010, ApJ, 725, 1405
Burrows, A., & Liebert, J. 1993, RvMP, 65, 301
Burrows, A., Marley, M., Hubbard, W. B., et al. 1997, ApJ, 491, 856
Capistrant, B. K., Soares-Furtado, M., Vanderburg, A., et al. 2024, AJ, 167, 54
Carrera, R., Bragaglia, A., Cantat-Gaudin, T., et al. 2019, A&A, 623, A80
Chabrier, G., Baraffe, I., Phillips, M., & Debras, F. 2023, A&A, 671, A119
Choi, J., Dotter, A., Conroy, C., et al. 2016, ApJ, 823, 102
Crepp, J. R., Principe, D. A., Wolff, S., et al. 2018, ApJ, 853, 192
Curtis, J. L., Agüeros, M. A., Douglas, S. T., & Meibom, S. 2019, ApJ, 879, 49
Curtis, J. L., Agüeros, M. A., Matt, S. P., et al. 2020, ApJ, 904, 140
Cutri, R. M., Wright, E. L., Conrow, T., et al. 2013, Explanatory Supplement to the AllWISE Data Release Products, AllWISE
Cutri, R. M., Wright, E. L., Conrow, T., et al. 2021, yCat, 2328, 0
De Furio, M., Faherty, J. K., Bardalez Gagliuffi, D. C., et al. 2025, ApJL, 990, L63
Dicken, D., Marín, M. G., Shivaei, I., et al. 2024, A&A, 689, A5
Dotter, A. 2016, ApJS, 222, 8
Douglas, S. T., Agüeros, M. A., Covey, K. R., & Kraus, A. 2017, ApJ, 842, 83
Douglas, S. T., Curtis, J. L., Agüeros, M. A., et al. 2019, ApJ, 879, 100
Dupuy, T. J., & Liu, M. C. 2017, ApJS, 231, 15
Eikenberry, S., Elston, R., Raines, S. N., et al. 2004, SPIE, 5492, 1196
Eikenberry, S., Elston, R., Raines, S. N., et al. 2008, SPIE, 7014, 70140V
Fabricius, C., Luri, X., Arenou, F., et al. 2021, A&A, 649, A5
Faherty, J. K., Burgasser, A. J., Walter, F. M., et al. 2012, ApJ, 752, 56
Faherty, J. K., Burningham, B., Gagné, J., et al. 2024, Natur, 628, 511
Faherty, J. K., Riedel, A. R., Cruz, K. L., et al. 2016, ApJS, 225, 10
Filippazzo, J., Alejandro Merchan, S., & Cruz, K. 2025, sedkit, v2.1, Zenodo,
Filippazzo, J. C., Rice, E. L., Faherty, J., et al. 2015, ApJ, 810, 158
Foreman-Mackey, D., Hogg, D. W., Lang, D., & Goodman, J. 2013, PASP, 125, 306
Gagné, J. 2024, PASP, 136, 063001
Gagné, J., Mamajek, E. E., Malo, L., et al. 2018, ApJ, 856, 23
Gagné, J., Moranta, L., Faherty, J. K., et al. 2023, ApJ, 945, 119
Gaia Collaboration, Vallenari, A., Brown, A. G. A., et al. 2023a, A&A, 674, A1
Gaia Collaboration, Vallenari, A., Brown, A. G. A., et al. 2023b, A&A, 674, A1
Gaidos, E., Mann, A. W., Lépine, S., et al. 2014, MNRAS, 443, 2561
Grimm, S. L., Malik, M., Kitzmann, D., et al. 2021, ApJS, 253, 30
Hargreaves, R. J., Gordon, I. E., Rey, M., et al. 2020, ApJS, 247, 55
Harris, C. R., Millman, K. J., van der Walt, S. J., et al. 2020, Natur, 585, 357
Hattori, S., Foreman-Mackey, D., Hogg, D. W., et al. 2022, AJ, 163, 284
Hegedűs, V., Mészáros, S., Jofré, P., et al. 2023, A&A, 670, A107
Hoch, K. K. W., Konopacky, Q. M., Theissen, C. A., et al. 2023, AJ, 166, 85
Høg, E., Fabricius, C., Makarov, V. V., et al. 2000, A&A, 355, L27
Hojjatpanah, S., Figueira, P., Santos, N. C., et al. 2019, A&A, 629, A80
Hunter, J. D. 2007, MCSE, 9, 90
Ishihara, D., Onaka, T., Kataza, H., et al. 2010, A&A, 514, A1
Jakobsen, P., Ferruit, P., Alves de Oliveira, C., et al. 2022, A&A, 661, A80
Jones, J., White, R. J., Boyajian, T., et al. 2015, ApJ, 813, 58
Kirkpatrick, J. D., Cushing, M. C., Gelino, C. R., et al. 2011, ApJS, 197, 19
Kirkpatrick, J. D., Martin, E. C., Smart, R. L., et al. 2019, ApJS, 240, 19
Kirkpatrick, J. D., Gelino, C. R., Faherty, J. K., et al. 2021, ApJS, 253, 7
Koposov, S., Speagle, J., Barbary, K., et al. 2024, Zenodo,
Kumar, S. S. 1963, ApJ, 137, 1121
Lacy, B., & Burrows, A. 2023, ApJ, 950, 8
Leggett, S. K., & Tremblin, P. 2024, RNAAS, 8, 13
Leggett, S. K., Morley, C. V., Marley, M. S., & Saumon, D. 2015, ApJ, 799, 37
Leggett, S. K., Tremblin, P., Phillips, M. W., et al. 2021, ApJ, 918, 11
Line, M. R., Teske, J., Burningham, B., Fortney, J. J., & Marley, M. S. 2015, ApJ, 807, 183
Liu, M. C., Dupuy, T. J., & Ireland, M. J. 2008, ApJ, 689, 436
Luhman, K. L., Tremblin, P., Alves de Oliveira, C., et al. 2024, AJ, 167, 5
Luo, Y., Németh, P., Deng, L., & Han, Z. 2019, ApJ, 881, 7
Madhusudhan, N., Harrington, J., Stevenson, K. B., et al. 2011, Natur, 469, 64
Mainzer, A., Bauer, J., Grav, T., et al. 2011, ApJ, 731, 53
Markwardt, C. B. 2009, ASPC, 411, 251

Marley, M. S., Saumon, D., Visscher, C., et al. 2021, ApJ, 920, 85
Marocco, F., Eisenhardt, P. R. M., Fowler, J. W., et al. 2021, ApJS, 253, 8
Marocco, F., Kirkpatrick, J. D., Schneider, A. C., et al. 2024, ApJ, 967, 147
Meibom, S., Barnes, S. A., Platais, I., et al. 2015, Natur, 517, 589
Meisner, A. M., Leggett, S. K., Logsdon, S. E., et al. 2023, AJ, 166, 57
Morley, C. V., Mukherjee, S., Marley, M. S., et al. 2024, ApJ, 975, 59
Mukherjee, S., Fortney, J. J., Morley, C. V., et al. 2024, ApJ, 963, 73
Mukherjee, S., Mang, J., Wogan, N., et al. 2025, Zenodo,
Öberg, K. I., Murray-Clay, R., & Bergin, E. A. 2011, ApJL, 743, L16
Paxton, B., Bildsten, L., Dotter, A., et al. 2011, ApJS, 192, 3
Paxton, B., Cantiello, M., Arras, P., et al. 2013, ApJS, 208, 4
Paxton, B., Marchant, P., Schwab, J., et al. 2015, ApJS, 220, 15
Paxton, B., Schwab, J., Bauer, E. B., et al. 2018, ApJS, 234, 34
Phillips, M. W., Tremblin, P., Baraffe, I., et al. 2020, A&A, 637, A38
Phillips, M. W., Liu, M. C., & Zhang, Z. 2024, ApJ, 961, 210
Pinfield, D. J., Jones, H. R. A., Lucas, P. W., et al. 2006, MNRAS, 368, 1281
Popinchalk, M., Faherty, J. K., Curtis, J. L., et al. 2023, ApJ, 945, 114
Prochaska, J. X., Hennawi, J. F., Westfall, K. B., et al. 2020a, JOSS, 5, 2308
Prochaska, J. X., Hennawi, J., Cooke, R., et al. 2020b, pypeit/PypeIt: v1.0.0,
    Zenodo, doi:10.5281/zenodo.3743493
Prochaska, J. X., Hennawi, J. F., Westfall, K. B., et al. 2020c, JOSS, 5, 2308
Rebull, L. M., Stauffer, J. R., Bouvier, J., et al. 2016, AJ, 152, 113
Ricker, G. R., Winn, J. N., Vanderspek, R., et al. 2015, JATIS, 1, 014003
Rickman, E. L., Ségransan, D., Hagelberg, J., et al. 2020, A&A, 635, A203
Rothermich, A., Faherty, J. K., Bardalez-Gagliuffi, D., et al. 2024, AJ,
    167, 253

Rothman, L. S., Gordon, I. E., Barber, R. J., et al. 2010, JQSRT, 111, 2139
Saumon, D., & Marley, M. S. 2008, ApJ, 689, 1327
Saumon, D., Marley, M. S., Abel, M., Frommhold, L., & Freedman, R. S.
    2012, ApJ, 750, 74
Schneider, A. C., Cushing, M. C., Kirkpatrick, J. D., et al. 2015, ApJ, 804, 92
Skilling, J. 2004, AIPC, 735, 395
Skilling, J. 2006, AIPC, 872, 321
Skrutskie, M. F., Cutri, R. M., Stiening, R., et al. 2006, AJ, 131, 1163
Smart, R. L., Tinney, C. G., Bucciarelli, B., et al. 2013, MNRAS, 433, 2054
Speagle, J. S. 2020, MNRAS, 493, 3132
Steinmetz, M., Guiglion, G., McMillan, P. J., et al. 2020, AJ, 160, 83
Suárez, G., Faherty, J. K., Burningham, B., et al. 2025, ApJ, 993, 165
Suárez, G., Metchev, S., Leggett, S. K., Saumon, D., & Marley, M. S. 2021,
    ApJ, 920, 99
Taylor, M. B. 2005, ASPC, 347, 29
Tennyson, J., Yurchenko, S. N., Zhang, J., et al. 2024, JQSRT, 326, 109083
Van-Lane, P. R., Speagle, J. S., Eadie, G. M., et al. 2025, ApJ, 986, 59
Virtanen, P., Gommers, R., Oliphant, T. E., et al. 2020, NatMe, 17, 261
Wright, E. L., Eisenhardt, P. R. M., Mainzer, A. K., et al. 2010, AJ, 140, 1868
Xuan, J. W., Hsu, C.-C., Finnerty, L., et al. 2024, ApJ, 970, 71
Yurchenko, S. N., Barber, R. J., Tennyson, J., Thiel, W., & Jensen, P. 2011,
    JMoSp, 268, 123
Zhang, Z., Liu, M. C., Claytor, Z. R., et al. 2021a, ApJL, 916, L11
Zhang, Z., Liu, M. C., Marley, M. S., Line, M. R., & Best, W. M. J. 2021b,
    ApJ, 916, 53
Zhang, Z., Mukherjee, S., Liu, M. C., et al. 2025, AJ, 169, 9